7 The retrieval of snow characteristics from optical measurements

Alexander A. Kokhanovsky and Vladimir V. Rozanov

7.1 Introduction

Retrievals of snow grain size using ground/satellite optical measurements have been performed by several research groups (Bourdelles and Fily, 1993; Fily et al., 1997; Zege et al., 1998; Polonsky et al., 1999; Nolin and Dozier, 1993, 2000; Nolin and Liang, 2000; Painter et al., 1998, 2003; Stamnes et al., 2007; Hori et al., 2007; Zege et al., 2008; Lyapustin et al., 2009). The aim of this chapter is to discuss the information content of corresponding measurements and also to present the fast semi-analytical snow grain size retrieval algorithm.

Retrievals are based on the fact that the snow reflectance in the near-IR (say, above 800 nm) decreases for larger particles because larger grains are relatively more absorptive as compared to smaller grains. Actually the same physical mechanism is used for the optical sizing of droplets/grains in cloudy media. The retrievals for snow fields are complicated by the fact that corresponding pixels can be contaminated by forest, soil, vegetation, or slash. Also snow horizontal (e.g., sastrugi) and vertical (e.g., buried ice/dust layers) inhomogeneity can bias retrievals.

In addition, the determination of the concentration c of pollutants in snow is discussed. The value of c can be assessed from measurements in the UV and visible, where pure snow reflects almost 100% of incident radiation and polluted snow absorbs a significant portion of light. The effect of absorption leads to snow darkening, which can be accurately measured and used for the determination of concentration of pollutants (at least, for heavy pollution events).

7.2 Forward model

In most snow retrieval algorithms it is assumed that snow can be modeled as an ice cloud layer positioned on the ground. Therefore, snow reflectance can be derived from the solution of the corresponding radiative transfer equation. In particular, if the assumption of a semi-infinite snow layer is used, then the Ambartsumian nonlinear integral equation can be used for studies of radiative transfer in snow (Mishchenko et al., 1999). The parameters of this equation are the single

scattering albedo ω_0 and phase function $p(\theta)$ (θ is the scattering angle). Alternatively, other radiative transfer solvers (e.g., SCIATRAN (www.iup.physik.uni-bremen.de/sciatran)) can be used assuming a large value of snow optical thickness (say, 5000). The single scattering albedo can be calculated as (Kokhanovsky and Nauss, 2005):

$$\omega_0 = 1 - \beta \quad , \tag{1}$$

$$\beta = \beta_\infty (1 - \exp(-\alpha\ell)). \tag{2}$$

Here β is the probability of photon absorption (PPA), $\alpha = 4\pi\chi/\lambda$ is the temperature-dependent bulk ice absorption coefficient, χ is the imaginary part of the ice refractive index at the wavelength λ. This formula was obtained fitting geometrical optics results derived with the Monte Carlo code described by Macke et al. (1996). The value of β_∞ corresponds to the limiting case of an ice crystal which absorbs all radiation penetrating inside the particle ($\alpha\ell \to \infty$). It can be calculated using the model of spherical particles because total reflection from an impenetrable sphere and a randomly oriented non-spherical impenetrable convex particle coincides (van de Hulst, 1957). It follows that $\beta_\infty = 0.47$ at the refractive index $n = 1.31$ (for ice in the visible). The particle absorption length (PAL) ℓ is proportional (Kokhanovsky and Nauss, 2005) to the effective grain size (EGS) $a_{ef} = 3V/\Sigma$ (V is the average volume of grains and Σ is their average surface area):

$$\ell = K a_{ef} \tag{3}$$

with the parameter K *depending on the shape of particles.* For weakly absorbing particles, it follows from Eqs. (2), (3) that:

$$\beta = \beta_\infty K \alpha a_{ef}. \tag{4}$$

We found using geometrical optics Monte Carlo simulations and fitting procedure implemented in ORIGIN that $K = 2.63$ for fractals and, therefore, $\beta = D\alpha a_{ef}$ with $D \approx 1.24$.

The phase function was modeled using the assumption of fractal grains (Macke et al., 1996) (see Fig. 7.1, where other possible snow phase functions are given as well). It is assumed that the phase function does not depend on the size of grains. This is a correct assumption in the geometrical optics domain, if particles are not absorbing (outside diffraction peak). The assumption of spherical particles is not very realistic and must be discarded (Tanikawa et al., 2006; Xie et al., 2006).

7.3 The information content of snow spectral reflectance

7.3.1 Theory

The radiance I over a snow field as detected on a satellite depends on the snow properties and also on atmospheric parameters in the propagation channel. The snow parameter of interest in this work is the effective grain size. The retrievals of EGS can be effected by the concentration of pollutants (CP) c. Therefore, it is of importance to derive both parameters simultaneously. So here we will study the sensitivity of the reflection function to the determination of both EGS and CP.

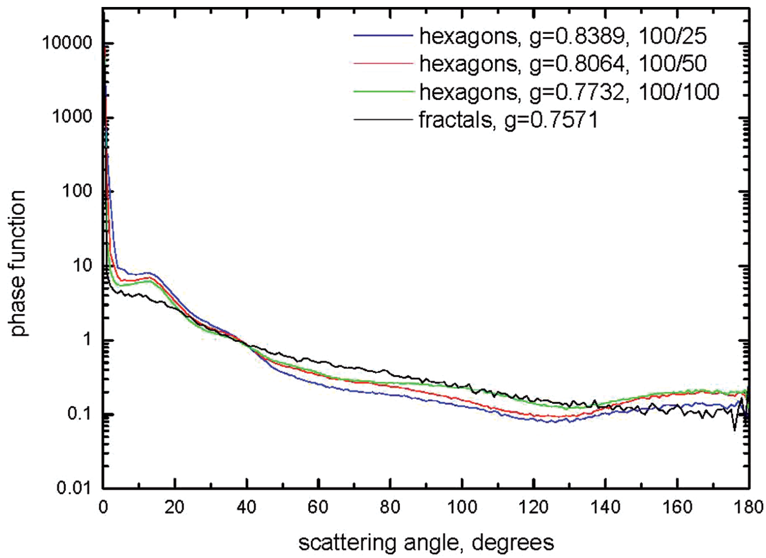

Fig. 7.1. The dependence of the phase function on the shape of particles. The following shapes were considered: hexagons with the length to the diameter ratios equal to 100/25, 100/50, 100/100 micrometers and fractal particles (Macke et al., 1996) at the wavelength 550 nm (Kokhanovsky et al., 2011). The diameter is defined as the distance between opposite sides of the hexagon. For all particles the surface was assumed to be rough in the calculations. The asymmetry parameter g is given for each curve. It follows that these diverse shapes do not produce very different phase functions as is the case for spheres, where the reduced scattering in the side-scattering region (around 90°) takes place. Also glories and rainbow characteristics of spheres are not observed for irregularly shaped particles.

The derivatives of the snow reflectance defined as

$$R = \frac{\pi I}{\mu_0 E_0} \tag{5}$$

($\mu_0 = \cos\vartheta_0, \vartheta_0$ is the solar zenith angle (SZA), E_0 is the incident light irradiance) with respect to these parameters are given by:

$$D_a = \frac{\partial R}{\partial a_{ef}}, \quad D_c = \frac{\partial R}{\partial c}. \tag{6}$$

They help to understand if given measurements can be used to retrieve the pair (a_{ef}, c). Clearly, derivatives depend on the viewing and illumination geometry (solar zenith angle (SZA) ϑ_0, viewing zenith angle (VZA) ϑ, and the relative azimuthal angle (RAA) φ), the spectral channel, values of (a_{ef}, c), and also on the atmospheric conditions (primarily through the aerosol optical thickness (AOT) τ). So, quite generally, we can write:

$$D = f\big(\vartheta_0, \vartheta, \varphi, \lambda, a_{ef}, c, \tau\big). \tag{7}$$

The task of this section is to understand how the derivatives D_a and D_c are influenced by various parameters given in Eq. (7). For this we use the software code

SCIATRAN (http://www.iup.uni-bremen.de/sciatran/). The derivatives are calculated through the following chain of equations.

First of all the weighting function (WF) W is introduced. We define it as (e.g., in the case of WF, W_a for a_{ef} of a homogeneous snow layer):

$$W_a = \frac{\partial R}{\partial \ln a_{ef}} = a_{ef} D_a. \tag{8}$$

Clearly, this is a dimensionless quantity. Then, it follows, e.g., for the reflectance function at the effective radius a_{ef}:

$$R(a_{ef}) = R(\bar{a}_{ef}) + [a_{ef} - \bar{a}_{ef}] W_a / \bar{a}_{ef}, \tag{9}$$

if *a priori* assumed radius $\bar{a}_{ef}$ is close to a_{ef} (so the linear approximation is valid). Clearly, if $W_a = 0$, then the reflectance is not sensitive to a_{ef}. Similar equations can be written for WFs with respect to the concentration of impurities (W_c) and also AOT (W_τ). There are different ways to calculate weighting functions. One possibility is the numerical calculation of ratios $M = \Delta R / \Delta(\ln x)$, where x is equal to a_{ef}, c, or τ depending on the case considered. In SCIATRAN yet another approach for the calculation of derivatives is followed. It is faster as compared to the calculation of ratios M and also more accurate.

In particular, it is assumed that the variation of the reflectance δR due to the variation of the effective radius profile $\delta a_{ef}(z)$ inside the snow layer of the thickness Hcan be presented in the following form:

$$\delta R(\lambda) = \int_0^1 w_a(\lambda, z) \delta a_{ef}(z)\, dz. \tag{10}$$

Here z is the vertical coordinate divided by the thickness of the layer$H$. It follows that the information on the function $w_a(\lambda, z)$ is of a great importance for understanding how changes in the profile $a_{ef}(z)$ influence the variation in reflectance. The WF W_a is related to $w(\lambda, z)$ via the following equation:

$$W_a(\lambda, z) = w_a(\lambda, z) a_{ef}(z). \tag{11}$$

Then it follows that:

$$\delta R(\lambda) = \int_0^1 W_a(\lambda, z) \left[\delta a_{ef}(z)/a_{ef}(z)\right] dz \tag{12}$$

or

$$\delta R(\lambda) = \sum_{k=1}^{N_k} J_a(\lambda, z_k) \frac{a_{ef,k}(z) - \bar{a}_{ef,k}(z)}{\bar{a}_{ef,k}(z)}, \tag{13}$$

where the summation is performed for the number of layers N_k inside of snow layer specified in the input of SCIATRAN and

$$J_a(\lambda, z_k) = W_a(\lambda, z_k) \Delta z_k \tag{14}$$

are corresponding Jacobians related to the sub-layer of thickness Δz_k. For a homogeneous layer it follows that:

$$\delta R(\lambda) = [\delta a_{ef}/a_{ef}]\, W_a(\lambda, z) \tag{15}$$

and we return to the same expression as written above:

$$R(a_{ef}) = R(\bar{a}_{ef}) + \Delta R = R(\bar{a}_{ef}) + [a_{ef} - \bar{a}_{ef}]\, W_a/\bar{a}_{ef}. \tag{16}$$

The WF $W_a(\lambda, z_k)$ contains information not only on the dependence of R on a_{ef} but also on the sensitivity of the reflectance to the changes in the radii of grains at different layers inside the snow.

The derivatives

$$W_a(\lambda) = \sum_{k=1}^{N_k} J_a(\lambda, z_k) \tag{17}$$

and also Jacobians $J_a(\lambda, z_k)$ are the main parameters discussed in the next section. The corresponding derivatives and Jacobians with respect to the concentration of pollutants and AOT are also considered.

As follows from Eq. (13), W_a in Eq. (17) gives the change in the reflectance (δR) if the change in the radius is equal to 100%. The technique to derive $w_a(\lambda, z)$ using the solution of direct and adjoint radiative transfer equations is described by Rozanov et al. (2007).

7.3.2 Results

The results of numerical experiments on the sensitivity studies are shown in Figs. 7.2–7.9. Let us analyze them now. All results were obtained using SCIATRAN and assuming that snow can be modeled as an ice cloud with the optical thickness 5000 at the ground level (with fractal phase function shown in Fig. 7.1). It was assumed that snow impurities (soot) are present in the form of Rayleigh scatterers and they influence only absorption and not scattering processes in a snow layer. The LOWTRAN aerosol maritime model implemented in SCIATRAN with aerosol optical thickness $\tau(550\text{ nm}) = 0.05$ was used. Also molecular scattering (but not absorption) has been taken into account. SCIATRAN is able to simulate satellite signals to account for the gaseous absorption. However, this was not needed for this work because only channels almost free of gaseous absorption have been selected.

We show the dependence of Jacobians $J_c(\lambda, z)$ for soot concentration on the distance from the snow bottom for several wavelengths in Fig. 7.2. The top of snow layer is located at 1 m height. It follows that Jacobians are different from zero only in the upper snow layers. They are about zero at depths 20 cm (and larger) from the top in the visible. Therefore, the concentration of pollutants at very deep layers cannot be retrieved from satellite observations. The maximum of the sensitivity is at some distance from the top of the layer and then the sensitivity decreases with the distance from the top. Most sensitivity comes from the upper 5 cm of snow, if the visible channels are used. The penetration depth depends on the grain size, being greater for smaller grains. The sensitivity to soot concentration decreases with the wavelength and it happens more rapidly for larger snow grains (see, e.g., the blue

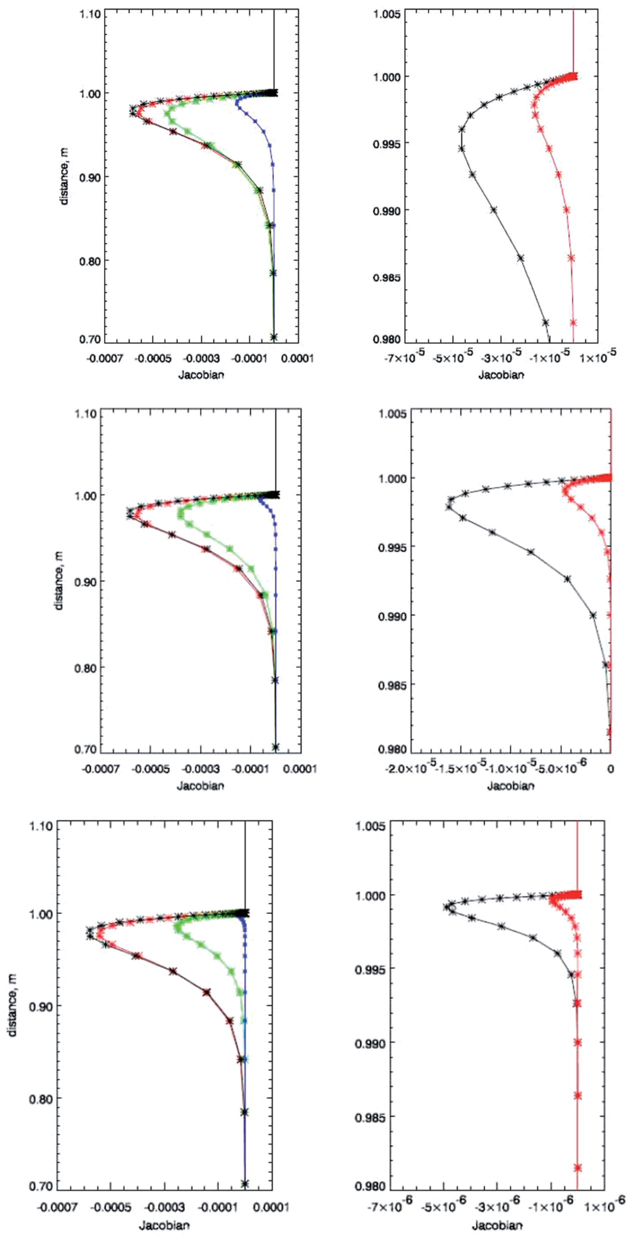

Fig. 7.2. Dependence of the Jacobian for soot concentration $J_c(\lambda, z)$ on the distance from the snow bottom at the wavelengths 400, 443, 555, 670 nm (left, larger Jacobians at maximum correspond to a smaller wavelength) and at wavelengths 865 and 1029 nm (right, larger Jacobians at maximum correspond to a smaller wavelength). The LOWTRAN aerosol model with the aerosol optical thickness (AOT) equal to 0.05 was used. The snow geometrical thickness is equal to 1 m and the length of side of fractal particles is equal to 50 micrometers (upper panel), 300 micrometers (middle panel), 750 micrometers (lower panel). The concentration of soot is equal to 10^{-8}. The solar zenith angle (SZA) is equal to 60 degrees and the observation is at the nadir direction.

line in Fig. 7.2). The main conclusion is that the shortest possible wavelength must be used for the soot concentration retrievals (e.g., at 400 nm). Then the dependence of retrievals on the grain size can be largely ignored (see Fig. 7.2).

Figure 7.3 is similar to Fig. 7.6 but now the Jacobians for the effective radius of snow grains are given. The green curves correspond to the measurements at 1240 nm. The upper panel of the figure corresponds to the case of $a_{ef} = 50$ μm. It follows that the use of 1240 nm channel is preferable (at least for the considered geometry). The channel at 1020 nm is the second choice (red line on the left plots). Channels located at 0.865, 1.61 and 2.2 μm can be used as well. The channel at 2.2 μm has slightly better performance (especially for large particles) as compared to the channel at 1.61 μm. The radiance in the 865–1240 nm range is sensitive just to the snow properties at the top (e.g., 5–10 cm from the top depending on the wavelength and also the size of particles; see Fig. 7.3, left panels). The radiance at 1610 nm and 2190 nm is sensitive to changes of the crystals' sizes only at a very top of the layer. As a matter of fact, the corresponding penetration depth is smaller than the EGS at these wavelengths (see right panels in Fig. 7.3). Therefore, retrievals in the spectral range 865–1240 nm range are most preferable with somewhat larger penetration depths (but smaller sensitivity) at 865 nm.

The dependence of the derivatives W_a, W_c, and W_τ on the wavelength is given in Fig. 7.4. The value of W_a is given by Eq. (17). The derivatives with respect to the concentration of a pollutant $c$and the aerosol optical thickness τ are defined in a similar way as for the value of a_{ef}. It follows from the analysis of this figure that the sensitivity to the soot concentration in snow disappears for larger wavelengths. This is generally the case for the aerosol optical thickness as well. The behavior of the derivative with respect to the grain size (at a fixed wavelength) is non-monotonous. At $a_{ef} = 50$ μm, the greatest sensitivity comes from the longer wavelengths. For the sizes of 300 and 750 μm, the greatest sensitivity comes from the wavelengths in the middle of the spectral interval studied (1.02 and 1.24 μm). Therefore, there is no such simple linear relationship to the wavelength in the sensitivity as in the case of the soot concentration. This is due to the fact that the influence of the size of grains on the reflectivity is small, both at low values of the absorption parameter $b = \alpha a_{ef}$ and also at high values of this parameter. Therefore, the optimum is located at some middle value of absorption, which occurs at 1240 nm for most practical situations. This also follows from the asymptotic radiative transfer theory. As it is shown by Kokhanovsky and Zege (2004) (see also the next section): $R \sim \exp(-\nu\sqrt{b})$ (ν is the parameter not depending on b) in the limit of weak light absorption by snow ($\beta \to 0$). This means that $W_a \sim \sqrt{b}\exp(-\nu\sqrt{b})$ and $W_a \to 0$ at high and low values of b as it was discussed above.

It follows that $W_\tau(\lambda) \ll W_a(\lambda)$ and, therefore, generally the information on AOT is of no importance for the grain size retrievals. This conclusion is valid only at AOT $= 0.05$ usual for clear polar conditions (Tomasi et al., 2007). The case of larger aerosol load (Arctic haze, for example) will be considered later on. Also we find that $W_c(\lambda) > W_\tau(\lambda)$ at channels 400 and 443 nm. Therefore, these channels can be used for the soot concentration determination. However, the influence of uncertainty in the value of AOT on the retrieval of soot concentration is much larger as compared to the case of a_{ef} retrieval. We conclude that without accurate retrievals of AOT, the retrievals of soot concentration in snow is not possible. The

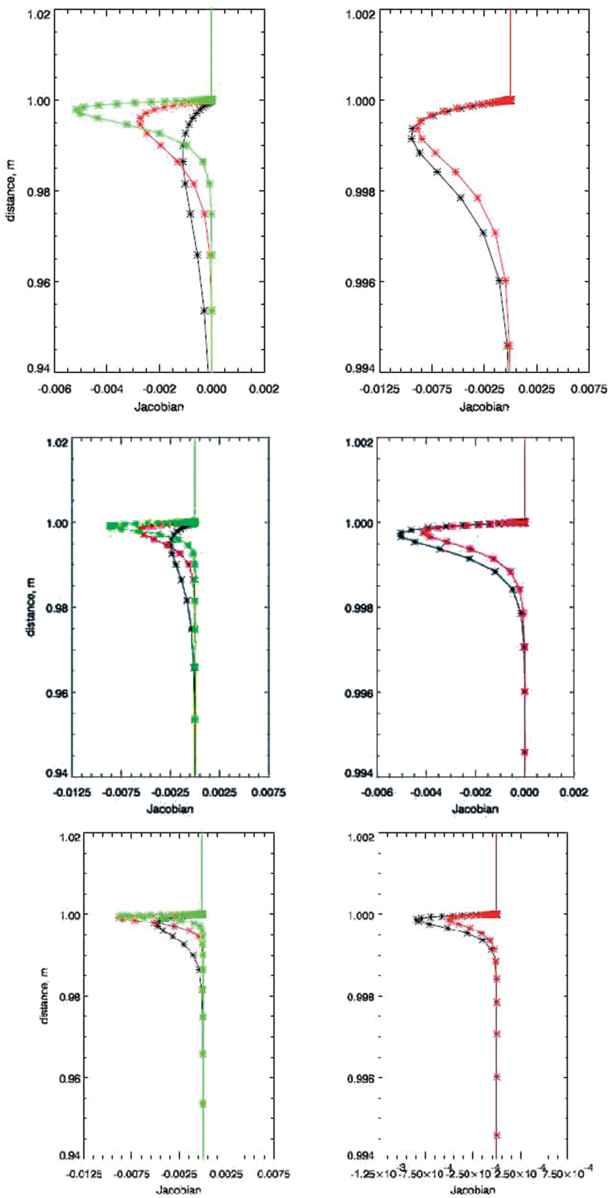

Fig. 7.3. Dependence of the Jacobian $J_a(\lambda, z)$ for effective radius of ice crystals in snow on the distance from the snow bottom at the wavelengths 865 nm (black curve), 1020 nm (red curve), and 1240 nm (green curve) (left panel). The same except at the wavelengths 1610 nm (red) and 2190 nm (black) (right panel). The LOWTRAN aerosol model with the aerosol optical thickness(AOT) equal to 0.05 was used. The snow geometrical thickness is equal to 1 m and the length of side of fractal particles is equal to 50 micrometers (upper panel), 300 micrometers (middle panel), 750 micrometers (lower panel). The concentration of soot is equal to 10^{-8}. The solar zenith angle (SZA) is equal to 60° and the observation is at the nadir direction.

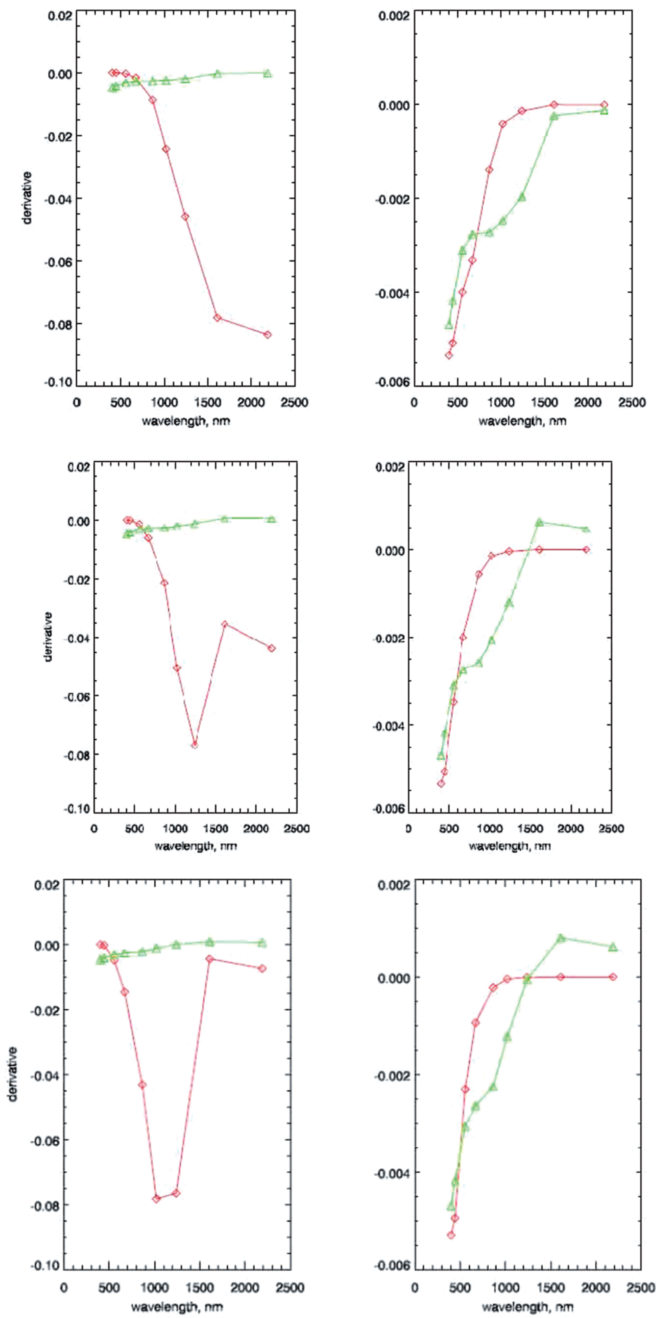

Fig. 7.4. Dependence of the derivatives W_a for effective radius (left, red curve) and W_c for the soot concentration (right, red curve) on the wavelength (AOT(555 nm) = 0.05). Other parameters are the same as in Fig. 7.3. Green lines give derivatives W_τ for the aerosol optical thickness at 555 nm.

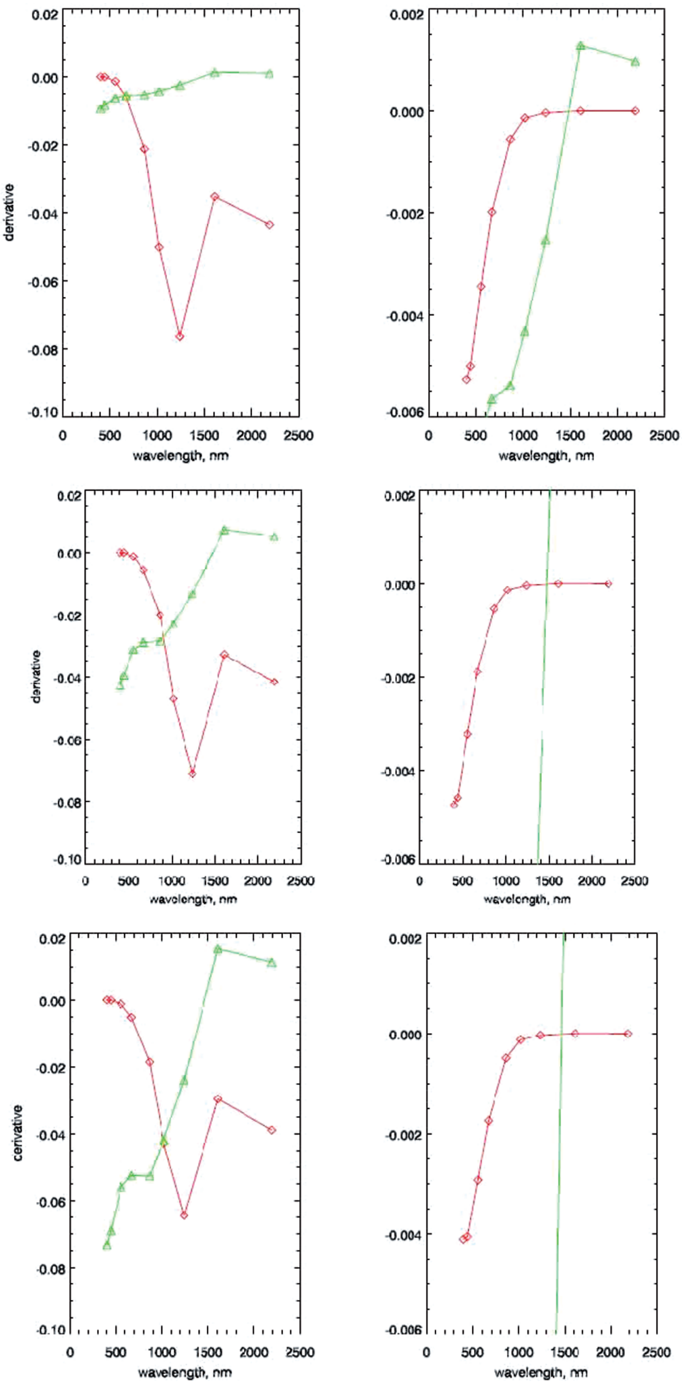

Fig. 7.5. The same as in Fig. 7.4 except at AOT = 0.1 (upper panel), 0.5 (middle panel), 1.0 (lower panel). The length side of fractal particles is 300 micrometers.

derivatives in Fig. 7.4 give the change in reflectance due to 100% change of a_{ef}, c, τ, respectively. We conclude that the signal at AOT = 0.05 is influenced in the similar way by the soot concentration in snow and the aerosol optical thickness. So accurate retrieval of AOT is of paramount importance for soot concentration determination. This is also confirmed by data shown in Fig. 7.5, which is similar to Fig. 7.4 except AOT = 0.1 (upper figures), AOT = 0.5 (middle figures), AOT = 1.0 (lower figures) are used in calculations. In all these cases (see figures on the right side) $W_c < W_\tau$ and, therefore, retrieval of soot concentration (at least at the level studied, $c = 10^{-8}$) is hardly possible without accurate information on aerosol optical thickness, which is difficult to retrieve over snow. As a matter of fact, both soot in snow and suspended aerosol particles can lead to the decrease of the registered signal and there is no technique in place to separation these two equally important contributions.

In Figs. 7.6–7.8 the dependence of derivatives on the viewing zenith angle, the solar zenith angle, and the relative azimuth, respectively, is presented. The main conclusion is that the viewing geometry influences grain size retrieval to a lesser extent as compared to the retrieval of soot concentration. Generally, retrieval of the

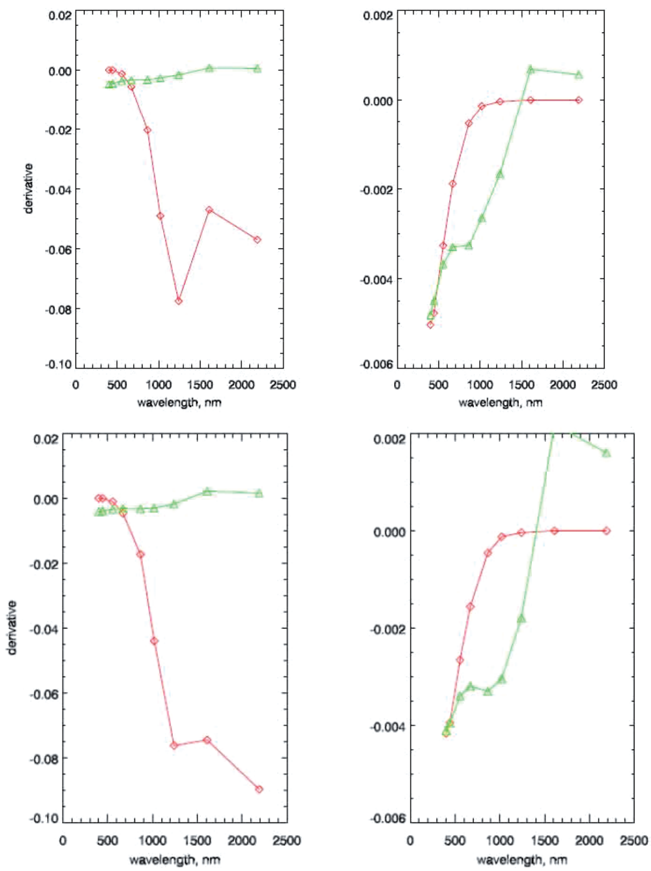

Fig. 7.6. The same as in Fig. 7.5 except at VZA = 25 (upper panel) and 50° (lower panel). The solar zenith angle is 60° and the relative azimuth is 0°.

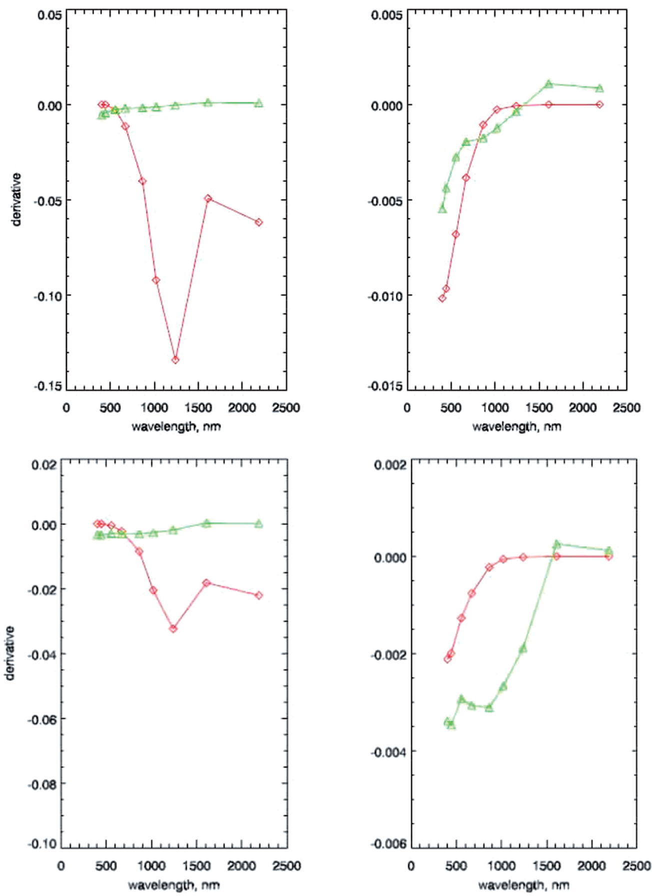

Fig. 7.7. The same as in Fig. 7.6 except at SZA = 45 (upper panel) and 75° (lower panel).

soot concentration is more problematic at larger VZAs due to long paths of light in the atmosphere. One cannotice (see Fig. 7.6) that the increase of VZA leads to the increase in the sensitivity to the EGS at wavelengths 1.6 and 2.1 μm. This is due to the fact that the snow brightness increases with VZA at these channels. Figure 7.7 shows the sensitivity of derivatives to the solar zenith angle. It follows that the sensitivity to the grain size increases for the high Sun. However, in the regions, where there is permanent snow cover and generally, where snowfalls occur, the Sun is low and the sensitivity to the grain size (and also the soot concentration) decreases considerably. For the solar zenith angle 45° (and also for smaller SZA), there is an enhanced sensitivity of measurements to the soot concentration. However, such high solar zenith angles usually do not occur in the snow-covered regions. The sensitivity to the soot concentration drops significantly at SZA = 75°. As follows from Fig. 7.8, the value of azimuth is also of importance as far as the sensitivity is of concern. The sensitivity is more pronounced at the relative azimuthal angle equal to zero degrees at the wavelengths 1.6 and 2.1 μm. For shorter wavelengths, the influence of the relative azimuthal angle on the sensitivity of retrievals is quite low.

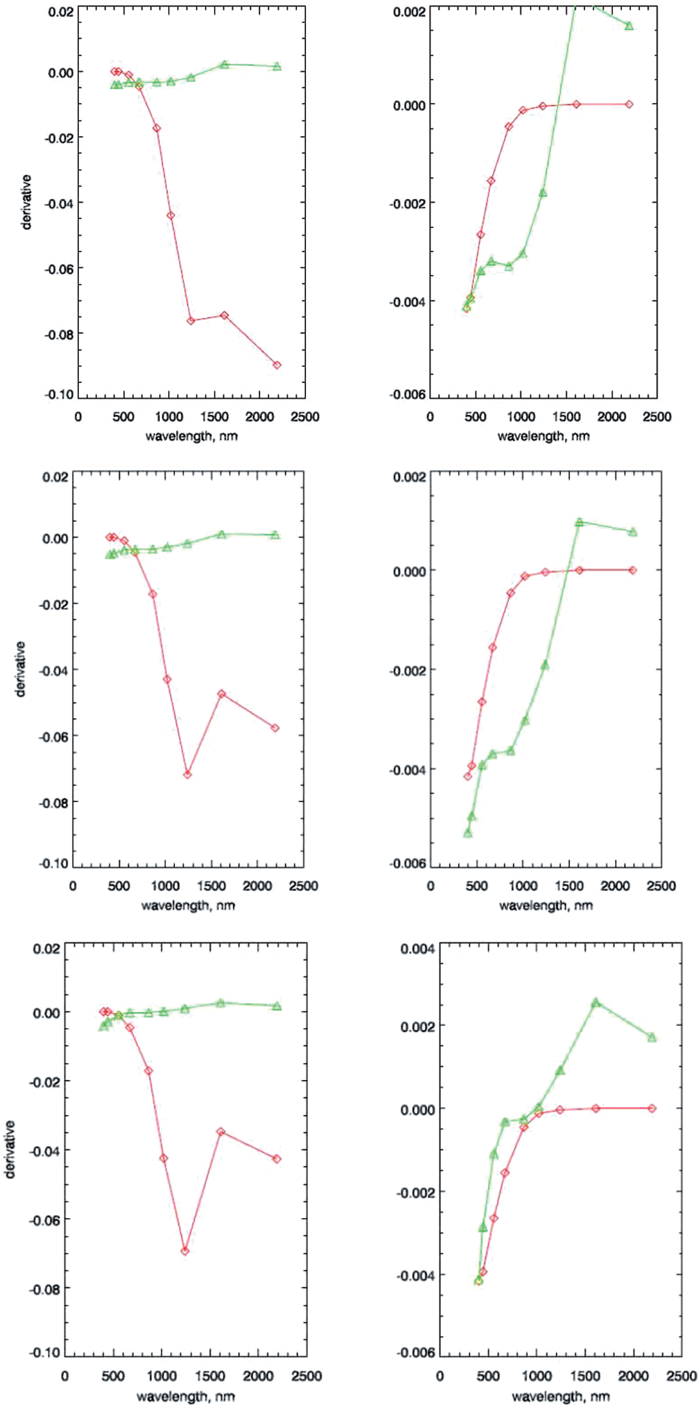

Fig. 7.8. The same as in Fig. 7.7 except at VZA = 50°, SZA = 60°, azimuths 0° (upper panel), 90° (middle panel) and 180° (lower panel).

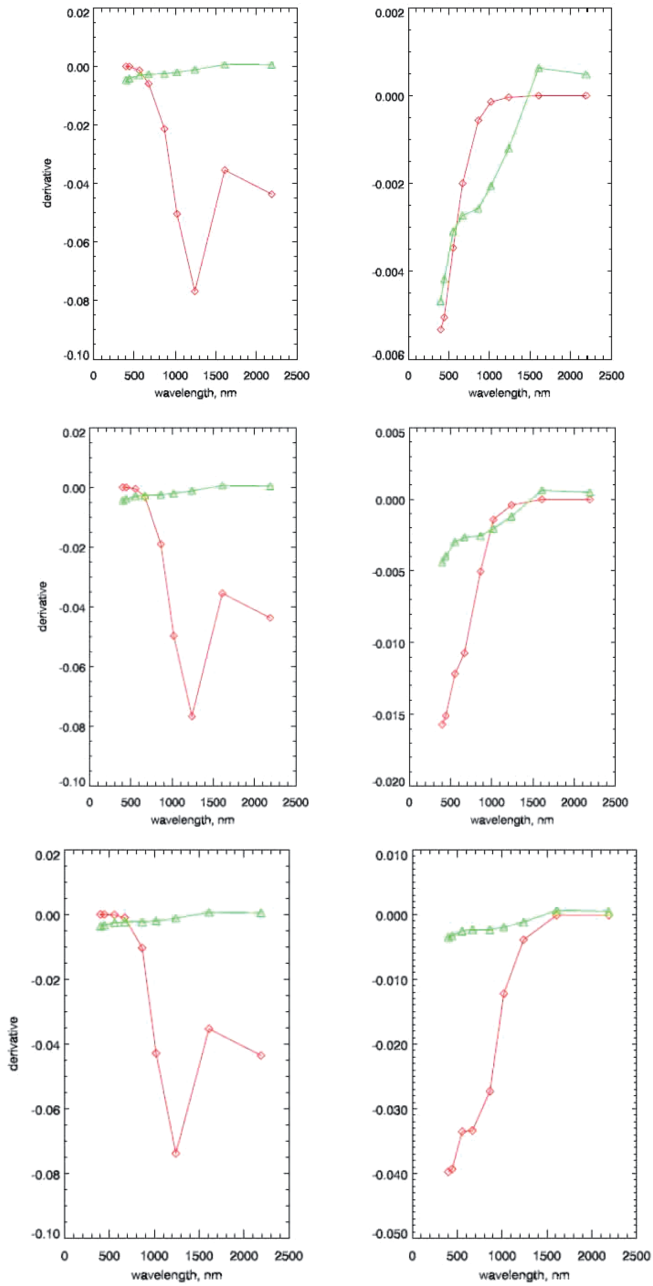

Fig. 7.9. Dependence of the derivatives W_a for effective radius (left, red curve) and W_c for the soot concentration (right, red curve) on the wavelength. Other parameters are as in Fig. 7.3. Green lines give derivatives W_τ for the aerosol optical thickness at 555 nm. The concentration of soot is equal to 10^{-8} (upper panel), 10^{-7} (middle panel), 10^{-6} (lower panel). The solar zenith angle (SZA) is equal to 60° and the observation is at the nadir direction. The length of side of fractal particles is equal to 300 micrometers.

All results shown above correspond to the background level of soot concentration ($c = 10^{-8}$). Clearly, for higher soot concentrations, the sensitivity of reflectance to the soot concentration is greater (see Fig. 7.9) and, therefore, c can be retrieved even if atmospheric correction is performed with considerable errors.

7.4 Retrieval algorithm: FORCE

7.4.1 Theory

The developed retrieval algorithm for the EGS determination is based on the look-up table (LUT) approach. In particular, the Fourier components of the reflection function in the visible (for a non-absorbing snow) are tabulated using the code developed by Mishchenko et al. (1999). The code solves the Ambartsumian nonlinear integral equation for the harmonics $R^m(\mu, \mu_0)$ of the reflection function. These harmonics are stored in LUTs. Then the reflection function at any relative azimuth angle is found as

$$R(\mu, \mu_0, \varphi) = R^0(\mu, \mu_0) + 2 \sum_{m=1}^{M_{\max}} R^m(\mu, \mu_0) \cos(m\varphi). \tag{18}$$

Here $\mu = \cos\vartheta$ and the value of $M_{\max}$ is chosen from the condition that the next term does not contribute more than 0.01% in the sum (18). In principle one more dimension (for a given phase function) in this LUT is needed and this is the dimension of the single scattering albedo.

We use the following representation valid as $\omega_0 \to 1$ (Zege et al., 1991; Kokhanovsky, 2006):

$$R(\mu, \mu_0, \varphi) = R_0(\mu, \mu_0, \varphi) A^{f(\mu, \mu_0, \varphi)}, \tag{19}$$

where

$$A = \exp\left\{-4s/\sqrt{3}\right\}, s = \sqrt{\frac{1-\omega_0}{1-g\omega_0}}, f = \frac{u(\mu_0)u(\mu)}{R_0^{-1}(\mu, \mu_0, \varphi)}, u(\mu) = \frac{3}{7}(1+2\mu). \tag{20}$$

Here R_0 is the reflection function of a semi-infinite snow layer under the assumption that the single scattering albedo is equal to one. It is calculated using Eq. (18). For pure snow, the experimentally measured value of R_0 (say, at 443 nm) can be used. This speeds up the retrievals.

The only approximation as compared to the exact RT calculations involved is the use of the term A^f in Eq. (19) to characterize light absorption by snow. The accuracy of this approximation is studied in Figs. 7.10–7.13. It follows that errors are below 6% as compared to SCIATRAN calculations at the wavelengths 0.52–1.24 μm and SZA = 54° for all azimuthal angles. So these short wavelengths will be used here for the inverse problem solution. In the case of MERIS onboard ENVISAT instrument (http://envisat.esa.int/instruments/meris/) channels 443 and 865 nm, the errors are smaller than 2% at the VZA < 40° typical for MERIS observations. This is well inside the calibration error of MERIS.

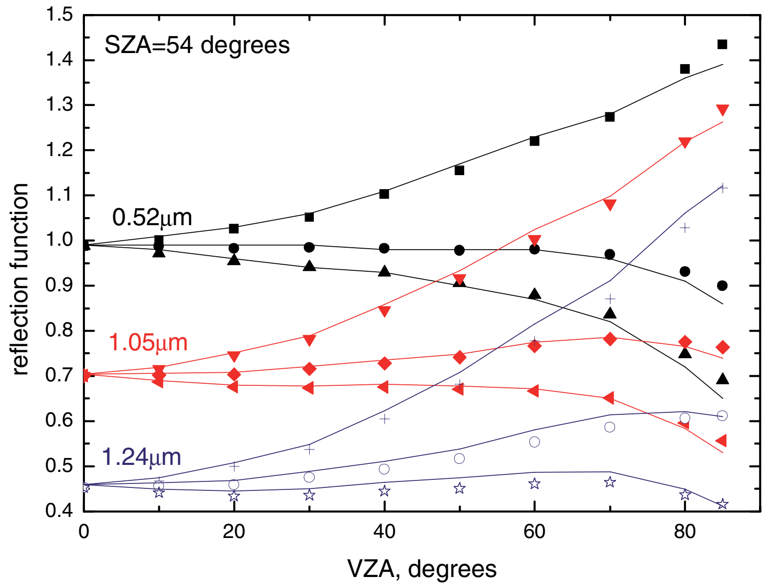

Fig. 7.10. The dependence of the reflection function on the viewing zenith angle (lines: approximate theory with the use of LUTs for the reflection function of a non-absorbing semi-infinite snow; points: SCIATRAN calculations) for selected wavelengths and the SZA equal to 54°. Lower lines for each wavelength correspond to the larger relative azimuthal angle equal to 0°, 90°, and 180°. The results are obtained using LUT for the function $R_0(\mu, \mu_0, \varphi)$ through the application of the nonlinear integral equation of Ambartsumian (Mishchenko et al., 1999).

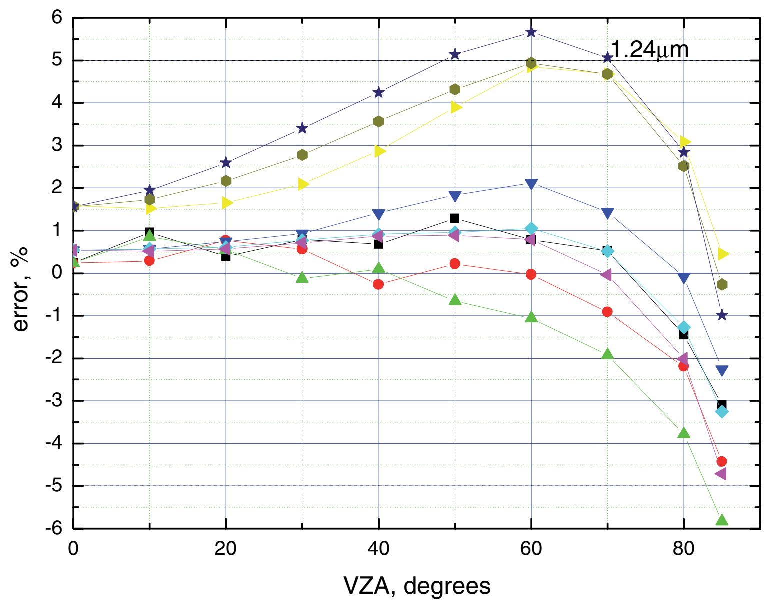

Fig. 7.11. Error of the approximation shown in Fig. 7.10. The upper curves correspond to the calculations at 1.24 μm. Lower curves correspond to calculations at 0.52 and 1.05 μm.

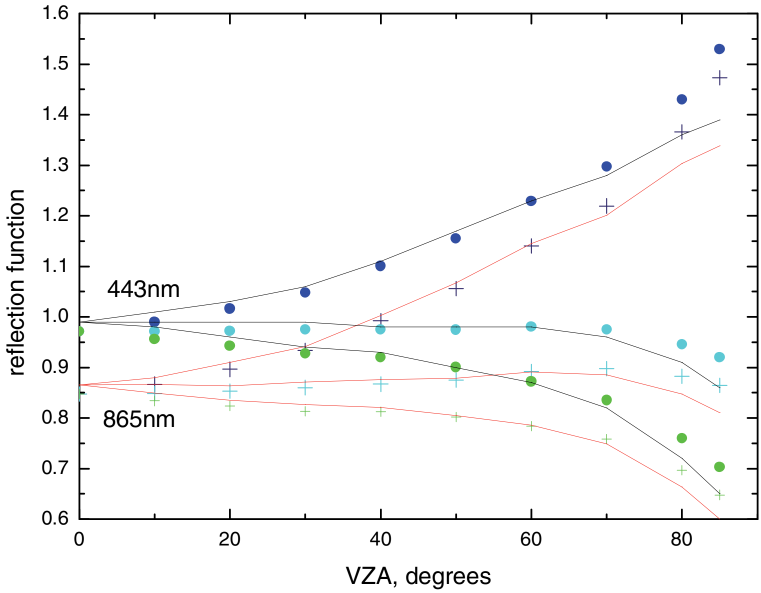

Fig. 7.12. The difference between reflectances at three azimuthal angles (0°, 90°, 180° from top down) at wavelengths 443 and 865 nm according to SCIATRAN (points) and the approximation (lines). The SZA is equal to 54°. SSA = 1 at the wavelength 443 nm. SSA = 0.9994 at the wavelength 865 nm. LUTs are used.

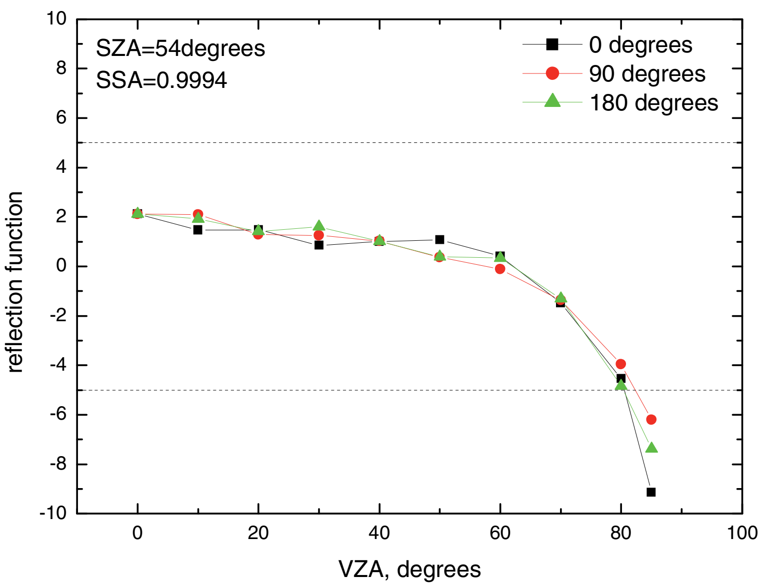

Fig. 7.13. Errors corresponding to the results shown in Fig. 7.12 at SSA = 0.9994 ($\lambda = 865$ nm).

MERIS does not have channels above 0.9 μm and, therefore, the approximation proposed here is very relevant to the interpretation of MERIS observations over snow fields. This is due to the fact that the snow albedo (and the accuracy of the approximation) increases for shorter wavelengths. The forward model itself (e.g., the flat snow surface assumption) and also errors of atmospheric correction introduce much larger errors as compared to differences between approximate and exact theories.

Eq. (19) can be used for the analytical determination of ω_0 and, therefore, a_{ef} from the snow reflection function measurements. As a matter of fact in the case of small grains and the MERIS wavelengths, even simpler approximation can be used. This approximation follows from Eq. (19) as $\omega_0 \to 1$:

$$R(\mu, \mu_0, \varphi) = R_0(\mu, \mu_0, \varphi) - \frac{4s}{\sqrt{3}} u(\mu) u(\mu_0). \tag{21}$$

Eq. (19) also enables the determination of the snow spectral albedo:

$$A(\lambda) = (R_{mes}(\lambda)/R_0)^{1/f} \tag{22}$$

from measurements of the spectral reflection function just at one observation geometry. It is assumed that the atmospheric correction has already been performed and the influence of atmosphere is removed from the value of $R_{mes}(\lambda)$.

One can write for channels 1(0.443 μm) and 2(0.865 μm) in the approximation under study:

$$R_1 = R_0 \exp(-\gamma \sqrt{\beta_1}), \tag{23}$$

$$R_2 = R_0 \exp(-\gamma \sqrt{\beta_2}), \tag{24}$$

where indices 1 and 2 signify the channel,

$$\gamma = \frac{4f}{\sqrt{3(1 - g\omega_0)}}. \tag{25}$$

We will neglect the difference of ω_0 from 1.0 in the denominator of Eq. (25).

Here we assume that there is some light absorption by snow even in the visible (e.g., due to soot). The value of probability of photon absorption can be written as

$$\beta = \frac{N_i C_{abs,i} + N_s C_{abs,s}}{N_i C_{ext,i} + N_s C_{ext,s}}. \tag{26}$$

Here

$$N_s = \frac{c_s}{\bar{V}_s} \tag{27}$$

is the number concentration of soot particles, $\bar{V}_s$ is their average volume, c_s is the volumetric concentration of soot (the fraction of volume filled by soot), $C_{abs,\alpha}$ is the average absorption cross-section of soot particles, $C_{ext,s}$ is the average extinction cross-section of soot particles. Parameters with the index 'i' have the same meaning as described above except for ice.

We will neglect the contribution of soot to the general light extinction in snow. Then it follows:

$$\beta = \beta_i + \beta_s, \tag{28}$$

where $\beta_i = C_{abs,i}/C_{ext,i}$ is given by Eq. (2) and

$$\beta_s = \frac{V_i c_s C_{abs,s}}{V_s c_i C_{ext,i}} \quad . \tag{29}$$

The average extinction cross-section of the ice grains $C_{ext,i}$can be estimated as follows (see Eqs. (3), (6)):

$$C_{ext,i} = \frac{\bar{\Sigma}_i}{2}. \tag{30}$$

Here $\bar{\Sigma}_i$ is the average surface area of grains. Taking into account that $C_{ext,i}/\bar{V}_i = 1.5a_{ef}^{-1}$ in this approximation and also assuming that $C_{abs,s}/\bar{V}_s = B\alpha_s$, which is true in the Rayleigh domain for small soot particles ($B = 0.84$ at the soot refractive index $n = 1.75$ (van de Hulst, 1957), $\alpha_s = 4\pi\chi_s/\lambda$, $\chi_s = 0.46$), we derive:

$$\beta_s = \frac{2}{3} Bc\alpha_s a_{ef} \tag{31}$$

where

$$c = c_s/c_i \tag{32}$$

is the relative soot concentration.

The mass absorption coefficient of soot $\sigma_{abs} = C_{abs}/\rho_s \bar{V}_s$ is equal to $B\alpha_s/\rho_s$ in the considered approximation. Here ρ_s is the soot density. Assuming that $B = 0.84$, $\chi_s = 0.46$, $\lambda = 443$ nm, $\rho_s = 1$ g/cm^3, one derives: $\sigma_{abs} = 8.4$ g/m^2, which is close to the modern estimates of this parameter (7.5 ± 1.2 m^2/g (Bond and Bergstrom, 2006; Flanner et al., 2007).

Therefore, we can write:

$$R_1 = R_0 \exp\left[-\gamma\sqrt{\frac{2}{3}B\alpha_{s,1}ca_{ef}}\right], \tag{33}$$

$$R_2 = R_0 \exp(-\gamma\sqrt{\beta_{i,2} + \frac{2}{3}B\alpha_{s,2}ca_{ef}}). \tag{34}$$

Here we neglected light absorption by ice at the first wavelength. These two equations can be used to find both the size of ice crystals and the concentration of pollutants. It follows from the first equation for $X = ca_{ef}$:

$$X = \frac{3}{2B\gamma^2\alpha_{s,1}} \ln^2 r_1 \tag{35}$$

and, therefore,

$$\beta_2 = \frac{\ln^2 r_2}{\gamma^2} - \frac{2}{3}BX\alpha_{s,2}, \tag{36}$$

where X is determined from Eq. (33). Here we introduced the normalized reflectance: $r_i \equiv R_i/R_0$. The EGS can be found from Eqs. (2), (3), (36):

$$a_{ef} = K\alpha_{i,2}^{-1} \ln\left[\frac{\beta_\infty}{\beta_\infty - \beta_2}\right]. \tag{37}$$

Then the concentration of soot is determined as $c = X/a_{ef}$. In practice, one measures the concentration of soot as the fraction of soot mass in a given mass of snow $c_f = c_s\rho_s/c_i\rho_i$, where ρ_s is the density of soot and ρ_i is the density of ice. Therefore, for the transformation of the satellite-derived c to the ground measured values of c_f, one must use the multiplier $\eta = \rho_s/\rho_i$:

$$c_f = \eta c. \tag{38}$$

We will assume that $\eta \equiv 1$ in this study. It is known that $\rho_i = 0.917$ g/cm^3. The density of soot depends on its structure. It varies in the range 1–2 g/cm^3. The assumption of $\eta \equiv 1$ is consistent with the lower limit of this variability.

For MODIS instrument (http://modis.gsfc.nasa.gov/about/), the channel at 1.24 μm is available in addition to 0.865 μm channel. The Global Imager (GLI, JAXA, currently not in operation) had several channels relevant to snow remote sensing (e.g., located at 0.865, 1.05 and 1.24 μm). The applications of the asymptotic radiative transfer theory for these sensors are given by Zege et al. (1998, 2008), Polonsky et al. (1999), Tedesco and Kokhanovsky (2007), and Lyapustin et al. (2009). The algorithms listed above differ from the algorithm presented here as follows:

- Zege et al. (2008) retrieval is based on the analysis of multiple channels (3 for MODIS (0.645,0.859,1.24) and 4 for GLI (0.68, 0.865, 1.05, 1.24). The obvious superiority of their technique is in the fact that uncertainty related to the modeling of R_0 can be substantially reduced due to the use of ratios of reflectances given by Eqs. (23), (24). The shortcomings are due to the fact that the algorithm is valid only for vertically homogeneous snow. Otherwise, the grain size is not constant along the vertical, and therefore, it differs at different channels due to different penetration depths. This effect is not taken into account by Zege et al. (2008).
- Lyapustin et al. (2009) propose two methods: one based on ratios of reflectivities at two close wavelengths, where light absorption by ice is not the same and another method actually very similar to the method described here. It is based on ratio of reflectivities at absorbing and non-absorbing bands. The first method can be applied only to the vertically homogeneous snow as correctly stated by Lyapustin et al. (2009). Therefore, they concentrate on the second method in the corresponding retrievals.
- The method of Tedesco and Kokhanovsky (2007) is based on a single wavelength measurement in the infrared. Therefore, the concentration of pollutants cannot be assessed and evaluated. The correspondence between different retrieval methods based on asymptotic theory is discussed in Appendix.

We note that in addition there are methods based on look-up tables of reflectivities. They produce similar results as methods discussed above if applied for similar setups and channels.

Generally, the wavelength 1.24 μm is the best for retrievals in the case of a homogeneous snow because then even heavy pollution does not influence the results of the grain size retrieval (therefore, one can put $X = 0$ in the expression for β_2 and derive the following simplified equation: $\beta_2 = \gamma^{-2} \ln^2 r_2$, which can be used in conjunction with Eq. (37) for the retrievals of a_{ef}). For vertically inhomogeneous snow, this wavelength brings information only from the top of the layer and may not be consistent with grains at deeper layers seen by the 443-nm wavelength used for the snow pollution retrieval. Even if measurements at 865 nm are used, there is quite large mismatch in the volume of snow sensed using 443 nm and 865 nm wavelengths. As follows from Figs. 7.6 and 7.7, the Jacobians for the soot concentration (at 443 nm) approach zero at the distance of 20 cm from the top layer and the values of Jacobians for the EGS vanish already 2–5 cm depending on the wavelength. Therefore, possible soot layer deposited at, say, 5 cm from the snow top will influence the signal in the visible but not at 865 nm. This makes application of the dual-wavelength algorithm not possible in this case and one should use the single channel algorithm outlined above.

7.4.2 Synthetic retrievals

To understand the sensitivity of the reflected radiation to the probability of photon absorption and the effective grain radius, we have performed a number of numerical experiments. In particular, we have implemented the retrieval algorithm in the numerical code and studied the influence of possible errors of forward model on the retrieval of PPA and a_{ef}. In particular, we have assumed that the measured reflectance differs by $\varsigma = \pm 5\%$ or $\pm 10\%$ from the forward model due to inherent calibration errors, errors of the forward model, cloud screening, atmospheric correction, etc. The resulting retrievals at the solar zenith angle equal to 54° and nadir observations are given in Fig. 7.14(a). It follows that the positive bias in the measured reflection function leads to underestimation of PPA (and otherwise for the negative bias). At $\varsigma = 0$, the algorithm retrieves input parameters with errors below several fraction of a percent (see the green line in Fig. 7.14(a)), which is the prove of the algorithm with the synthetic data. It follows from Figs. 7.14(b) that the error of PPA retrieval increases considerably as $\beta \to 0(\alpha a_{ef} \to 0)$. In particular, errors smaller than 20% (at a reasonable estimate of $\varsigma \sim 5\%$) are possible only if $\beta \geq 0.01$ ($\omega_0 \geq 0.99$). Therefore, it is of importance to use the spectral interval, where PPA varies in the range 0.01–0.02. The upper limit is needed to ensure small errors of the assumed asymptotic theory. It follows from Fig. 7.15 that the use of the wavelengths 1020 and 1240 nm is superior for the usually occurring grain sizes (0.05–1 mm). The value of ω_0 at $\lambda = 865$ nm is always smaller than 0.01 producing a reduced sensitivity to the effective grain radius. This is confirmed by Figs. 7.16(a) and (b), where we see that the value of $\varsigma = \pm 5\%$ makes retrievals at the wavelength 865nm possible with the accuracy better than 50% only at radii larger than 0.4 mm. Otherwise, retrievals are characterized by quite large errors. This is an unfortunate situation because the wavelength of 865 nm is the largest which can be used for retrievals using MERIS. The wavelengths of 885 and 900 nm are contaminated by the uncertainty in the water vapor vertical column and also they are not much different with respect to the sensitivity to the grain size retrievals

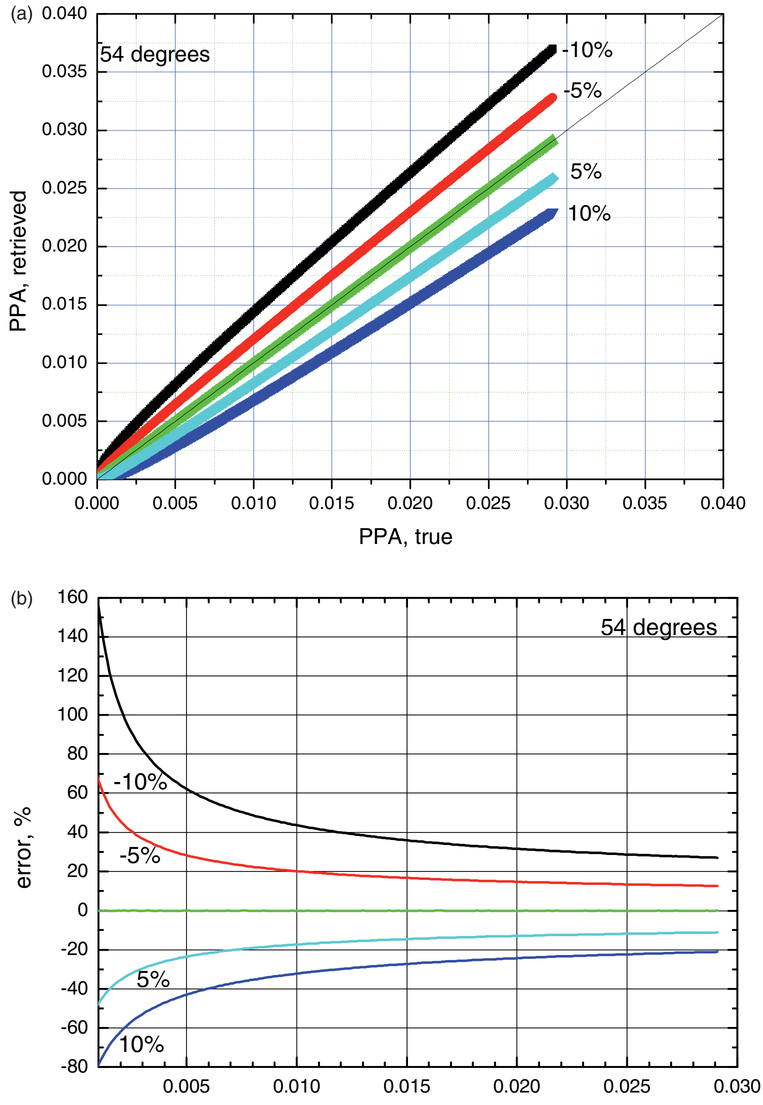

Fig. 7.14. (a) The retrieved PPA versus the assumed PPA at the incidence angle 54° and the nadir observations. (b) The error of the retrieved PPA versus the assumed PPA at the incidence angle 54° and the nadir observations.

as compared to the wavelength 865nm. At the wavelength 1020 nm, the errors of retrievals are smaller than 20%, if $\varsigma = \pm 5\%$at $a_{ef} \geq 0.2$ mm (see Fig. 7.17(a)). The errors reach maximum of 50% at $a_{ef} = 0.1$mm. The errors are still lower at 1240 nm (see Fig. 7.17(b)) but then the use of asymptotic theory is in question (at least for large sizes of grains).

The measurements at the wavelength 443 nm, where absorption of light by ice grains is small, can be used to retrieve the soot concentration in snow as described

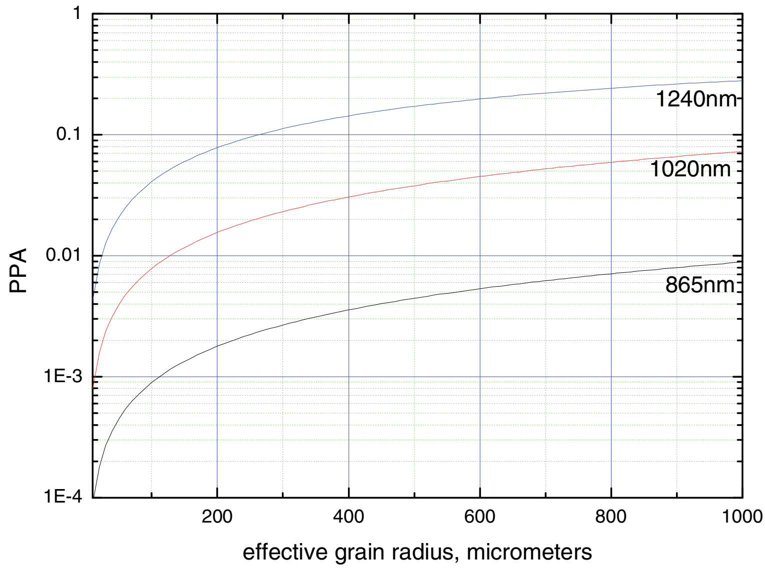

Fig. 7.15. The dependence of PPA on the effective grain radius.

above. To get the concentration of pollutants, one must determine grain size (at least for large grains). Errors in the determination of the grain size influence the retrieval of soot concentration. In particular, errors are large, if the concentration of pollutants is small. Then the retrieved values of β_s are not reliable. One can estimate β_s assuming that $c = 300$ ng/g, which is quite a high concentration of pollutants. Then $\beta = 0.0002$ at $a_{ef} = 0.1$ mm and 0.002 at $a_{ef} = 1$ mm. Clearly, these values of PPA are so small that the reliable determination of β and also $c \leq 300$ ng/g is hardly possible. And the values of the concentration above 300 ng/g are extremely rare (Hansen and Nazarenko, 2004; Flanner et al., 2007). Therefore, it is proposed to make retrievals of β (at 443 nm) only if the change of reflectance at this wavelength is considerable as compared to the case of pure snow. We show the difference of the calculated reflection functions of snow at PPA = 0.0002 and 0.002 in Figs. 7.18 at incident angles 54° and 75° as compared to the pure snow case. It follows that indeed retrievals at such levels of pollution are hardly possible due to errors of the forward model. The concentration of soot in the Arctic is just 10–30 ng/g (Flanner et al., 2007) and PPA is always smaller than 0.0002. Then the retrievals of soot concentration are doubtful. The comparison of retrievals with ground measurements also confirms this conclusion (Aoki et al., 2007).

Because the analytical dependence of the reflectance on relevant parameters is provided in the framework of our approach, it is also easy to calculate corresponding errors analytically. To simplify calculations, we use Eq. (19). Then after differentiation and some algebraic calculations, it follows for the uncertainty in the value of $b = \alpha a_{ef}$:

$$\frac{db}{b} = K_{amp}\frac{dR}{R}, \tag{39}$$

where the error amplification coefficient is given by the following equation:

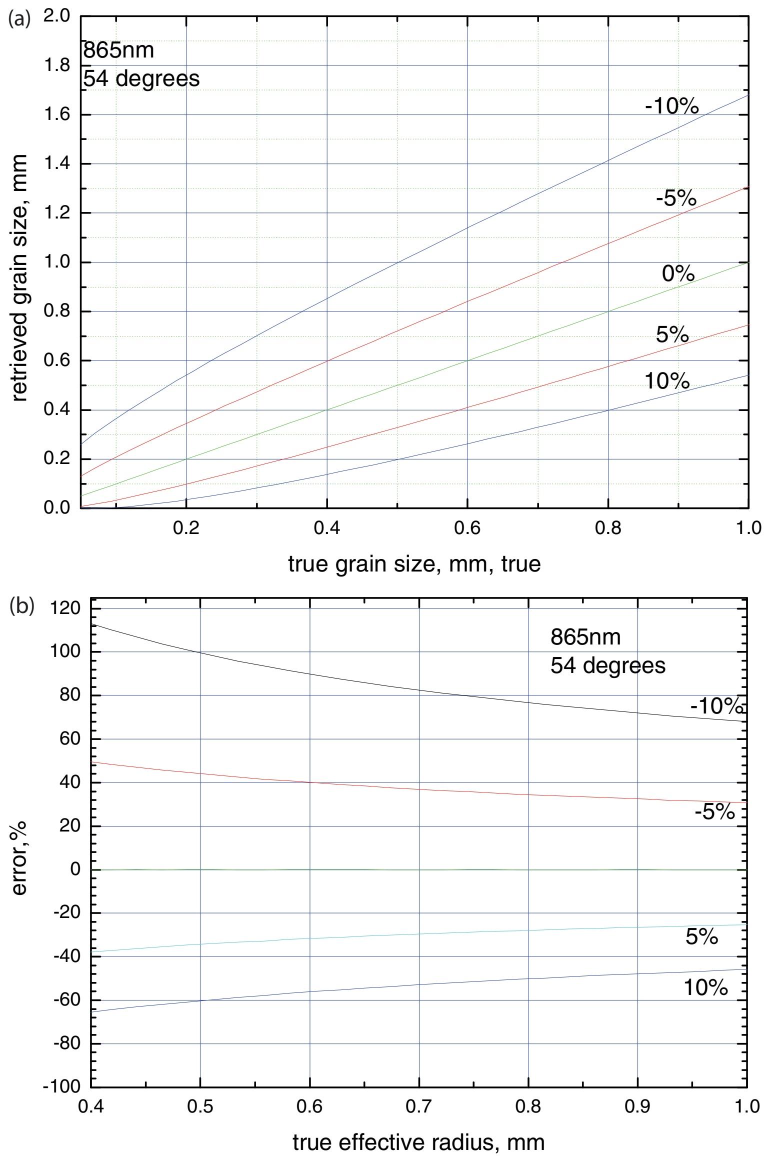

Fig. 7.16. (a) The retrieved effective grain radius versus the assumed grain radius at $\lambda = 865$ nm and SZA $= 54°$. (b) The error of the retrieved EGS as the function of the assumed effective radius of grains retrieved at $\lambda = 865$ nm.

$$K_{amp} = -\frac{2(R_0 - p\sqrt{b})}{p\sqrt{b}} \tag{40}$$

and

$$p = \frac{8Au(\mu)u(\mu_0)}{3\sqrt{3(1-g)}}. \tag{41}$$

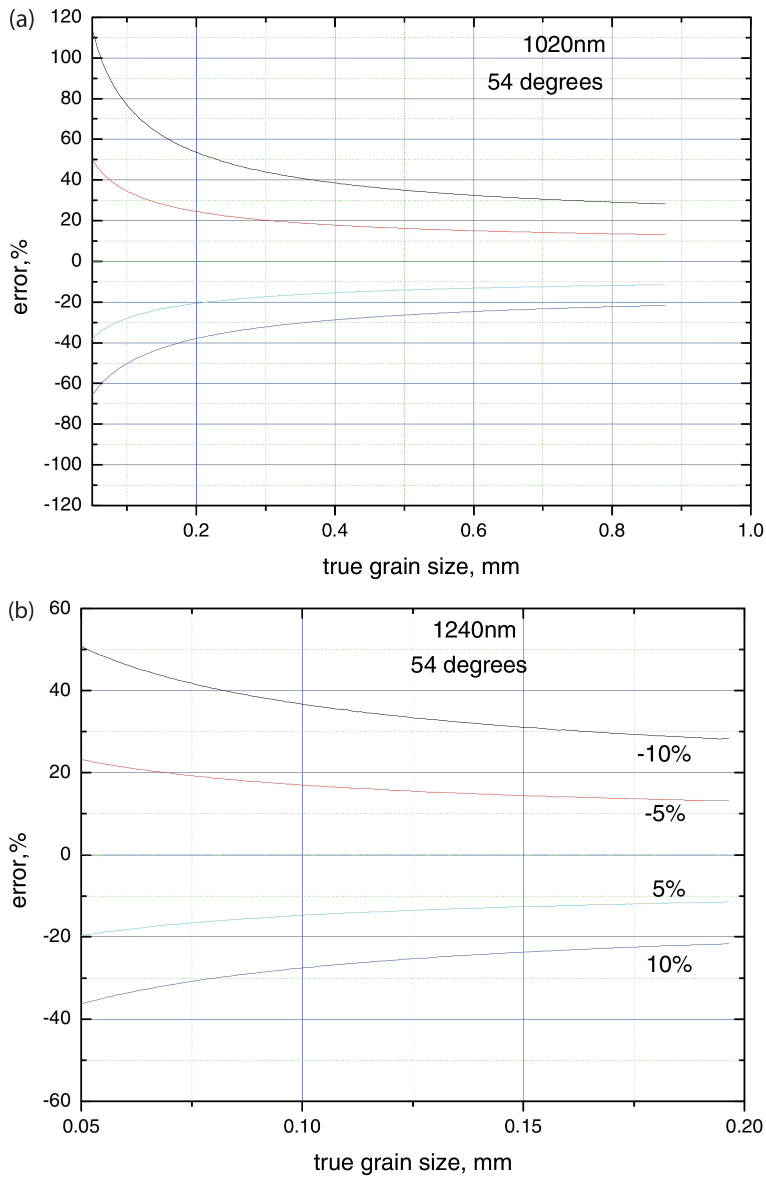

Fig. 7.17. (a) The error of retrieved EGS as the function of the assumed effective radius of grains at $\lambda = 1.02$ μm. (b) The error of the retrieved EGS as the function of the assumed effective radius of grains at $\lambda = 1.24$ μm.

The second term in the denominator of Eq. (40) can be neglected because it takes a small value in the approximation under study. It follows that $K_{amp} \to \infty$ as $b \to 0$, the finding which follows from the numerical experiment given above and also from the sensitivity study presented in the previous section. Because the function $u(\mu)$ increases with the cosine of the angle, we conclude that K_{amp}

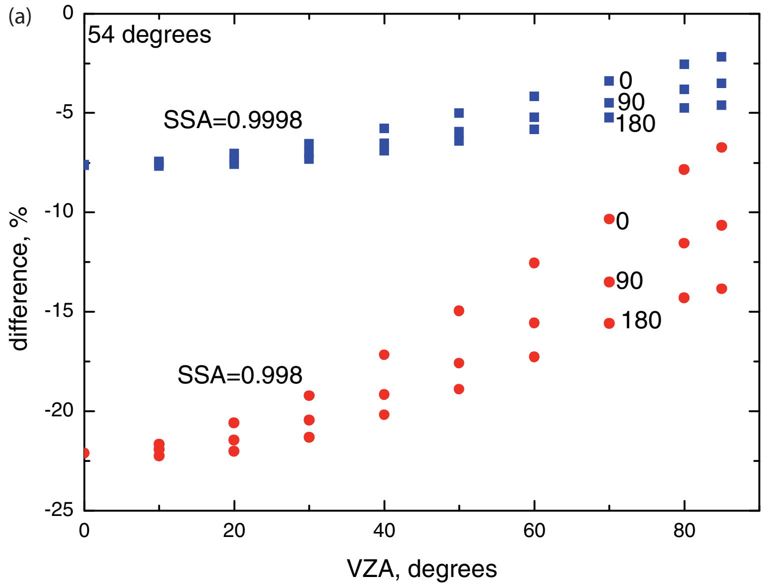

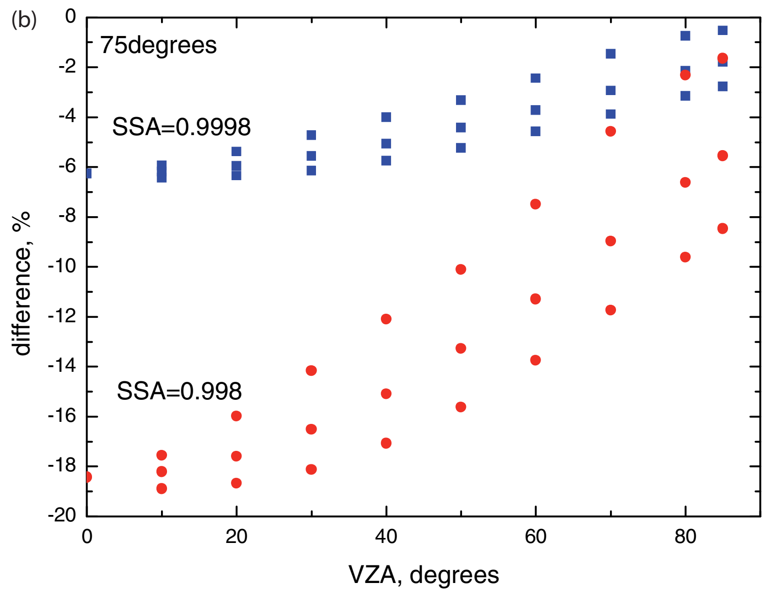

Fig. 7.18. (a) The difference of the reflection function from that for the case of a nonabsorbing snow as the function of the viewing zenith angle at azimuths 0°, 90°, and 180°, SZA = 54° (SSA = 0.998 and SSA = 0.9998). (b) The difference of the reflection function from that for the case of a nonabsorbing snow as the function of the viewing zenith angle at azimuths 0°, 90°, and 180°, SZA = 75° (SSA = 0.998 and SSA = 0.9998).

is somehow reduced for oblique observation and illumination conditions (at least for angular regions, where R_0 is constant or decreases, e.g., see cases with the RAA in the range 90–180°). The error amplification coefficient is proportional to $\sqrt{1-g}$ and, therefore, it is smaller as more extended in the forward direction phase functions.

7.4.3 Application of the algorithm to MERIS data

7.4.3.1 Atmospheric correction

As far as atmospheric correction over snow is concerned, we used the LUT of atmospheric reflectances calculated with SCIATRAN for a prescribed aerosol model. Anyway, the influence of atmosphere on grain size retrievals is small, as was proved in the sensitivity studies. Therefore, such an approach is well justified (at least for a clear atmosphere). In the case of polluted atmospheres, the atmospheric contribution must be assessed using measurements at the neighboring pixels containing open water or polynyas. We demonstrate the importance of atmospheric correction in Figs. 7.19 and 7.20, where results of SCIATRAN calculations are given for the case of surface albedo equal to 0.8 and overlying aerosol layer. It follows that the atmosphere substantially changes the values of reflectance as compared to the case $A = 0.8$ especially at large solar and viewing zenith angles and for shorter wavelengths. An interesting point to note is that the atmospheric contribution can increase or decrease the satellite signal over the snow field depending on the geometry and, therefore, relative contribution of the atmosphere to the signal.

The following simplified atmospheric correction algorithm is proposed. It is supposed that the correction for the gaseous absorption can be performed as:

$$R_{cor} = T_{gas} R_M, \tag{42}$$

where T_{gas} is the gaseous transmittance calculated as

$$T_{gas} = \exp(-\upsilon \mathrm{M}), \tag{43}$$

M is the trace gas vertical column (O_3, H_2O as obtained, e.g., from MERIS observations), $\upsilon = 1/\mu + 1/\mu_0$, R_M is the measured reflectance. The obtained reflectances R_{cor} (except at 760 and 900 nm channels) are corrected for Rayleigh and aerosol scattering using the pre-calculated LUTs. It is assumed that the aerosol optical thickness is equal to 0.05 (see, e.g., Tomasi et al., 2007) in the calculation of LUTs. The aerosol model is WMO coarse maritime aerosol model with no absorption assumed. The angle grid was one degree for SZA(0(1)89), VZA(0(1)80), and relative azimuth angle (0(1)180). Therefore, the largest possible mismatch of MERIS data and those in LUTs is 0.5°. The error due to this mismatch is smaller than 0.01 in the snow albedo, which is acceptable due to other complications inherent to snow properties retrievals. This is illustrated in Fig. 7.21, where we show the retrieved albedo (retrieved using the pre-calculated LUTs described above) under the assumption that true snow albedo is equal to 0.8. The synthetic data were generated not for the same grid as in LUT but for the 0.5-degree shifted LUT (for angles, the same shift was assumed). The algorithm performance is very good till VZA is equal

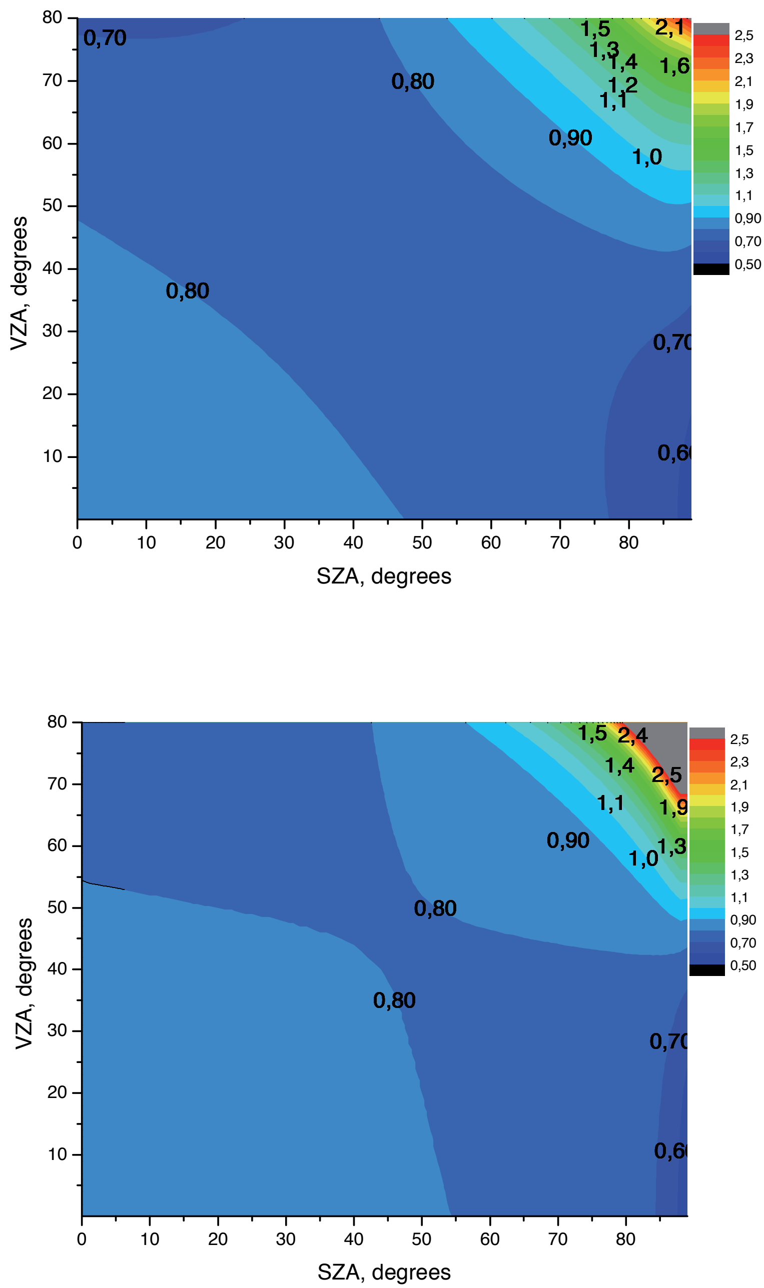

Fig. 7.19a. The dependence of the reflectance $R(443\text{ nm})$ (upper panel) and $R(865\text{ nm})$ (lower panel) on the SZA and VZA at the relative azimuth angle equal to 0.0. The case of the underlying Lambertian surface with albedo 0.8 is presented for the maritime coarse aerosol model with aerosol optical thickness equal to 0.05. The values of reflectance are above 0.8 in the lower left corner and well below 0.8 in the upper lower corner. This means that the Lambertian surface looks brighter from space, if observed from the nadir direction at SZA = 0.0. It looks darker for the nadir observation and the oblique solar light incidence (say, SZA = 80°).

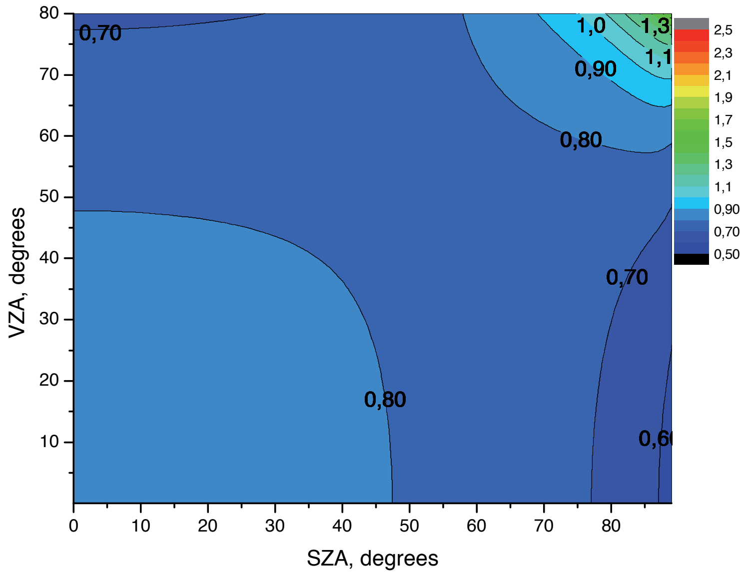

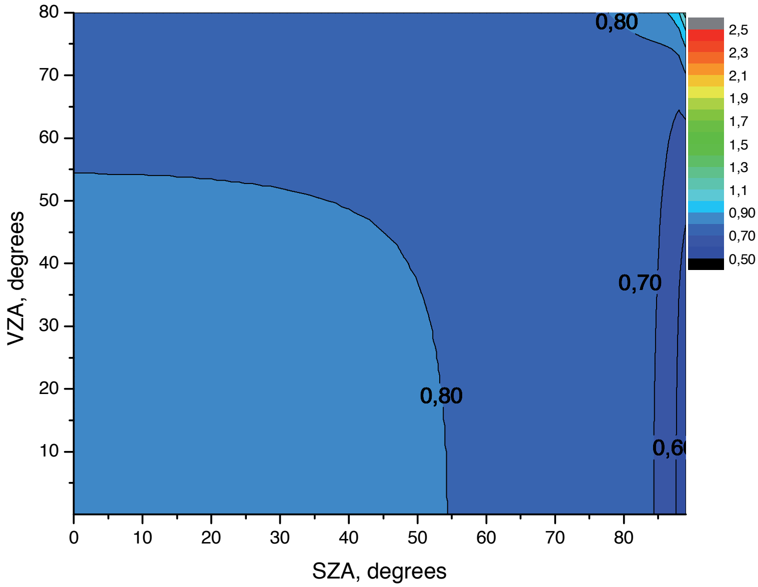

Fig. 7.19b. The same as in Fig. 7.19a except at RAA = 90°.

to 55°, which is of importance for AATSR measurements. The largest MERIS VZA is 42° and then the performance is even better. The true albedo is retrieved if no shift in the grid is applied and the same snow and atmosphere models are used in the solution of direct and inverse problems. The change of the aerosol model in the retrieval process (from maritime coarse to maritime fine) does not bring complications, if the aerosol optical thickness was assumed to be the same (0.05). It follows

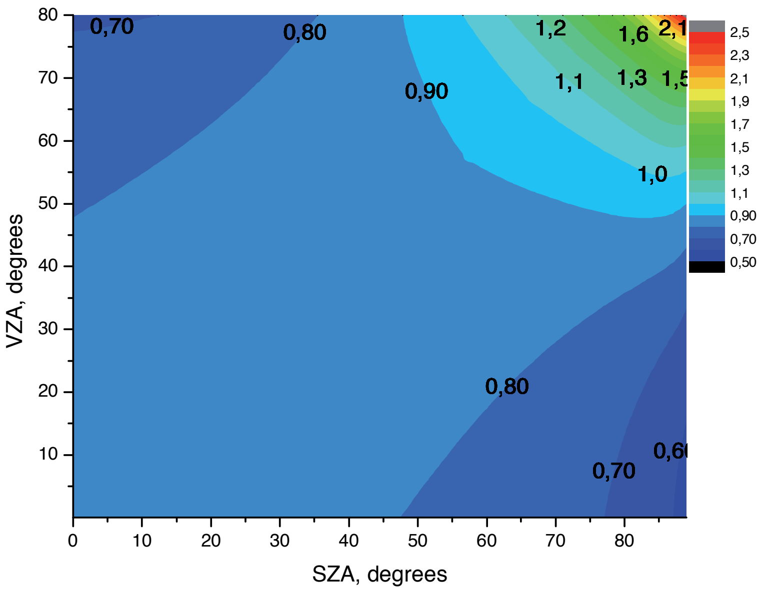

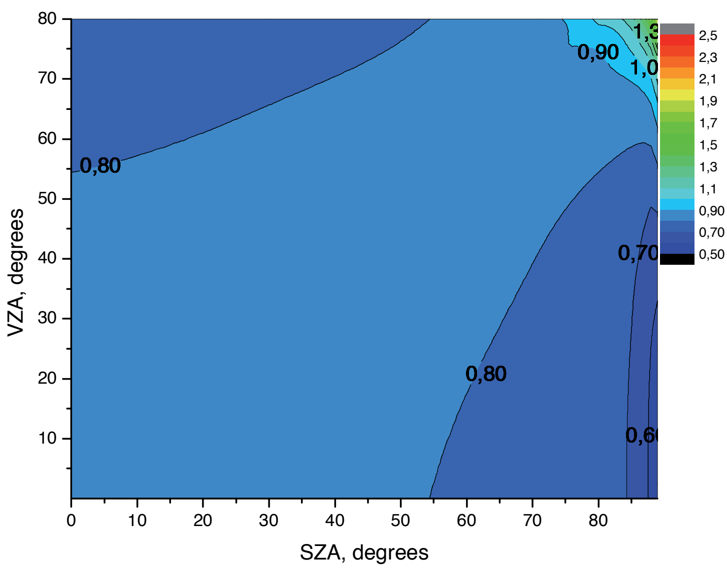

Fig. 7.19c. The same as in Fig. 7.19a except at RAA = 180°.

that errors of retrievals are negligible even in the case where the aerosol model is not correctly selected (the errors are less than 0.01 in the snow albedo) as far as MERIS observations are of concern (VZA < 42°).

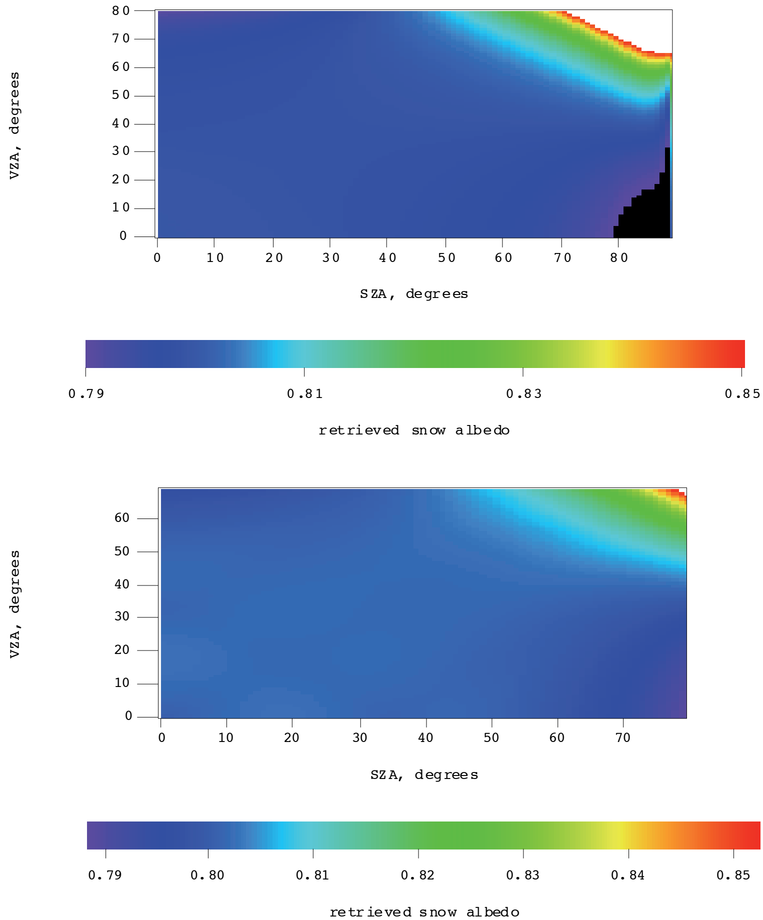

Fig. 7.20. The dependence of the reflectance of the snow field with the assumed Lambertian albedo 0.8 on the SZA. The vertical lines give the variability due the variation of the viewing zenith angle (0(1)80°) and relative azimuth (0(1)180°). The atmosphere can increase or decrease the albedo of the snow field depending on the geometry. The aerosol optical thickness is 0.05 and the coarse maritime aerosol model is assumed.

For the atmospheric correction, it is assumed that MERIS reflectance can be presented as

$$R = R_b + \frac{TR_s}{1 - Ar}. \tag{44}$$

Here R_b is the reflectance for a black underlying surface (stored in LUTs for molecular-aerosol atmosphere with the assumed aerosol optical thickness of 0.05 and coarse maritime aerosol model with no absorption), R_s is the snow reflectance, T is the atmospheric transmittance stored in LUTs, r is the spherical albedo stored in LUTs, $A = 0.8$ is the assumed snow albedo. The term Ar is quite small. Therefore, the assumption on A does not have a large impact on the retrieved snow reflectance:

$$R_s = (R - R_b)(1 - Ar)/T. \tag{45}$$

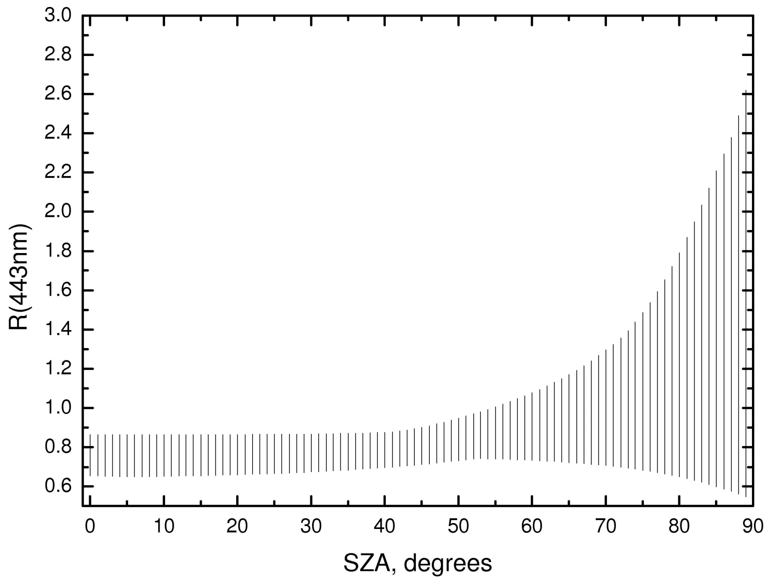

Fig. 7.21. The retrieved snow albedo as the function of the satellite and solar zenith angles. The aerosol optical thickness is equal to 0.05 and the fine-mode maritime aerosol phase function was used in synthetic data preparation. The relative azimuth was varied in the range 0(1)180°. The true snow albedo is equal to 0.8. The upper panel differs from the lower panel due to the different regions of change of SZA and VZA. The range of SZA and VZA change is lower in the figure shown at the bottom.

The algorithm described above is of importance only for MERIS channels below 800 nm, where the soot concentration and snow albedo is retrieved. The atmospheric correction is less important at 865 nm and also at 1020 and 1240 nm, where the snow grain size is usually retrieved.

7.4.3.2 The retrieval of snow grain size using MERIS observations

The MERIS browse image of the snow field under clear sky in Greenland is shown in Fig. 7.22. The corresponding maps of reflectances at 443 nm, and 865 nm, and also in the oxygen A-band (762 nm) are given in Fig. 7.23a and 7.23b. The line across the image in the case of measurements at 762 nm shows the border between two cameras of MERIS (the so-called instrumental smile effect).

A lot of clouds are present in the region. The retrieved grain size is shown in Fig. 7.24a and 7.24b (after atmospheric correction and cloud screening procedures have been applied). The average EGS is around 0.2 mm for the whole scene and 0.15 mm for the left part of the scene, Unfortunately, *in situ* data for EGS at this location during the satellite measurements are not available to us.

We show the results of the retrieved concentration of pollutants in Fig. 7.25 (in ng/g). The concentrations are very low as one might expect for Arctic. Generally, as follows from the sensitivity studies given above, the accurate determination of soot concentration from a satellite is difficult in the Arctic due to the low concentration

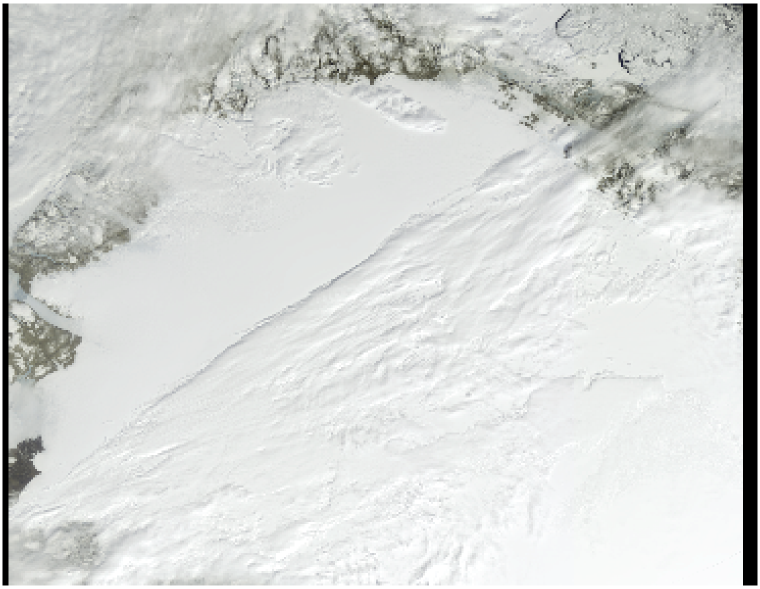

Fig. 7.22. Browse image of the scene analyzed. The retrievals have been performed for the clear sky portion of this image (Kokhanovsky et al., 2011).

of pollutants there. Although, as is seen from Fig. 7.19b, the magnitude of c is determined in a correct way.

7.5 Conclusions

In this work we discussed the snow grain size retrieval algorithm FORCE. The work is also relevant to the area of the determination of the specific area of snow using optical measurements (Schneebeli and Sokratov, 2004; Matzl, 2006; Matzl and Schneebeli, 2006; Gallet et al., 2009; Kokhanovsky and Schreier, 2009). The correlation coefficient between satellite and ground measurements of EGS is in the range 0.6–0.7. The small values of the correlation coefficient could be due to the different definitions of sizes in the ground and satellite measurements. Also we proposed techniques for the cloud screening and atmospheric correction of satellite images over snow. The algorithm must be improved in future. The current version of the algorithm was implemented in the ESA software package BEAM and free for use by the remote sensing community.

Several simplifications have been used in the algorithm development. In particular, it was assumed that snow is vertically homogeneous. In reality snow has a layered structure, as discussed by Colbeck (1991). The layering arises from a sequence of storms, reworking of the snow surface into a distinctive horizon which is subsequent buried, or the generation of certain types of horizons within the snow profile. Not only is the sequence of these buried layers unique from year to year and highly variable with location, but each layer also evolves as the snowy season progresses (Colbeck, 1982, 1983). Dust and soot can be deposited in such layers and

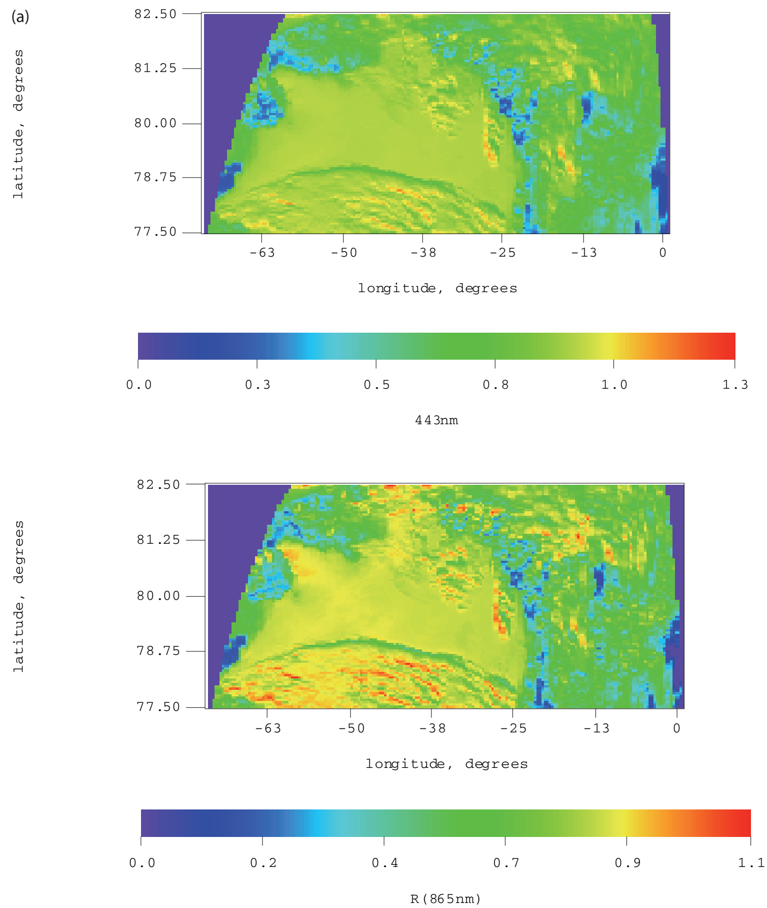

Fig. 7.23a. Maps of reflectances at 443 nm (upper panel) and 865 nm (lower panel) for the browse image shown in Fig. 7.22 (Kokhanovsky et al., 2011).

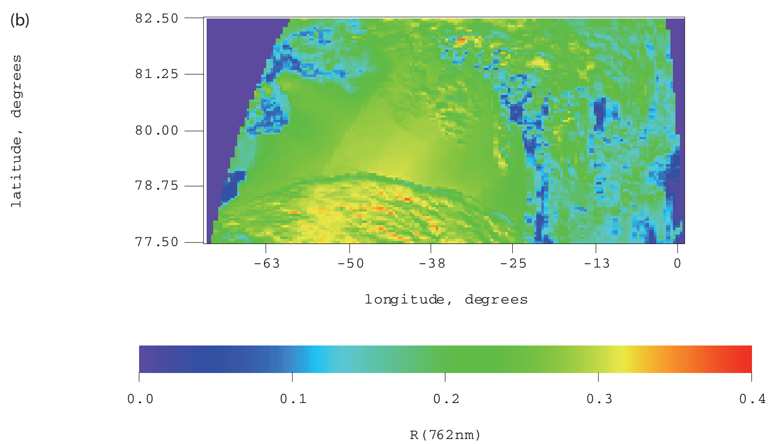

Fig. 7.23b. The map of reflectance at 762 nm (Kokhanovsky et al., 2011).

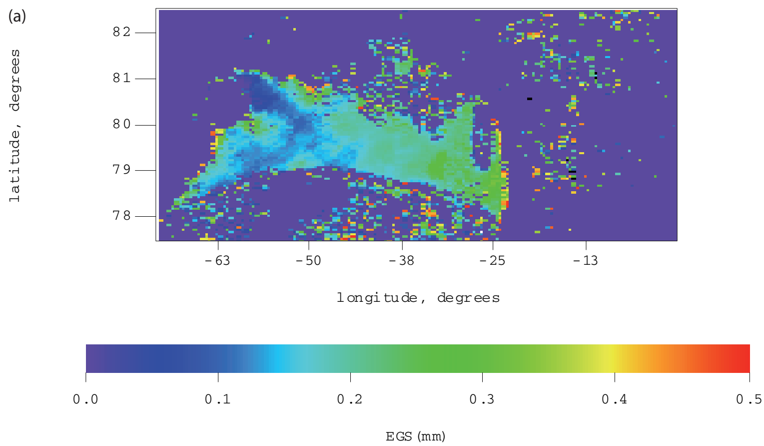

Fig. 7.24a. The retrieved snow grain size (Kokhanovsky et al., 2011).

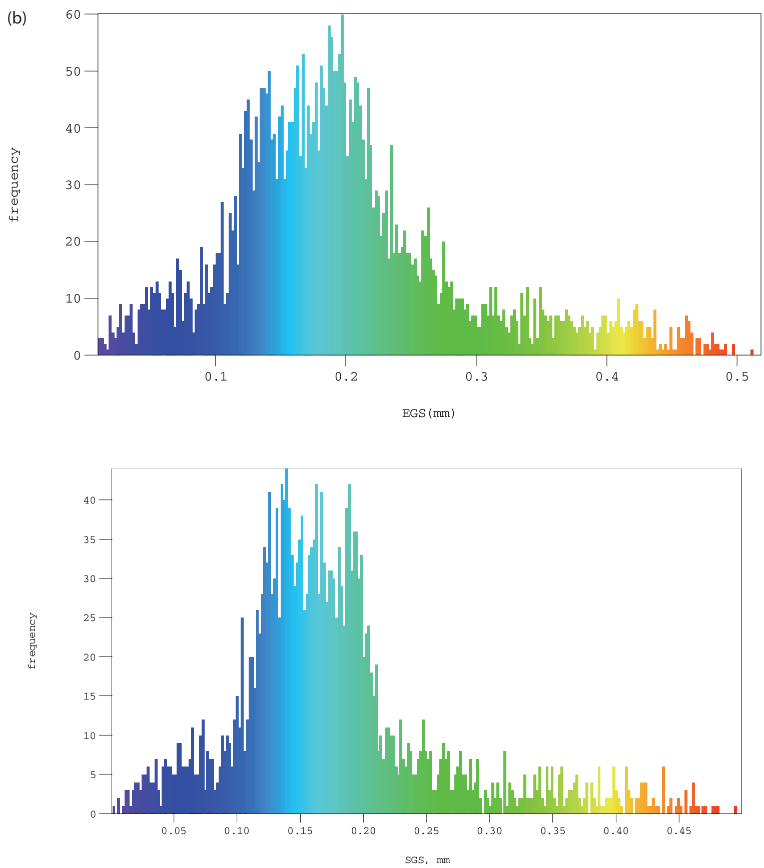

Fig. 7.24b. The retrieved snow grain size histogram (the lower panel corresponds to retrievals in the left part of the image) (Kokhanovsky et al., 2011).

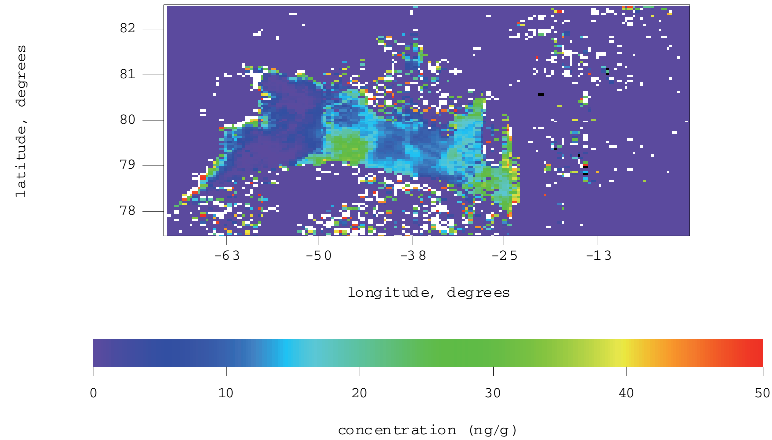

Fig. 7.25. The retrieved concentration of pollutants (Kokhanovsky et al., 2011).

then covered by the fresh snow. Because in standard retrieval algorithms vertically homogeneous snow is assumed, the pollutant content derived will be that of an entire snow column, which does not correspond to reality. Moreover, in retrievals one needs to assume the refractive index of the pollutants. The refractive index is considerably different for dust and soot. Also the absorption and scattering cross-sections of soot and dust particles are considerably different. Therefore, wrong *a priori* assumptions on the type of pollutants (soot, dust, red algae on the surface of snow) prevent correct retrievals of the concentration of pollutants. In principle, the type of pollutants can be distinguished from spectral measurements of the snow reflectance because, e.g., dust and soot have different spectral bulk absorption coefficients (e.g., red and gray colours). However, this is possible only in the case of thin covers of fresh snow over dirty snow or in the case of freshly polluted snow.

Also it follows that the structure of snow and also shapes/sizes of crystals are very different from the top to the bottom of the snow layer. This peculiarity is also not accounted for in the forward model. The snow grain size is retrieved using infrared measurements. But it is a well known fact that the imaginary part of the refractive index of ice changes with wavelength (and temperature). This means that light with different wavelengths will penetrate to different depths. Therefore, the use of multiple wavelengths, in principle, can reveal the vertical distribution of the snow grains (Li et al., 2001; Zhou et al., 2003). Using one-wavelength retrieval, only one grain size for a given depth is retrieved. Importantly, the snow penetration depth is not fixed for a given wavelength: it also depends on the grain size itself. Generally, it is lower for larger wavelengths. Therefore, it is of importance to report at which wavelength the retrievals have been performed. If pollution is not uniformly distributed in snow but rather contained in distinct layers (e.g., dust), then one cannot ignore light scattering by pollutants. Then both absorption and scattering effects by pollutants must be considered. Usually, in retrievals of EGS, the pollution is assessed assuming the homogeneous distribution of snow layer. If pollution is in a layer well below the snow surface, it plays no role in the EGS re-

trieval, but it can play some role if pollutants are close to the surface and retrievals are made at short wavelength (say 865 nm) and grains are small.

The radiative transfer models used extensively in the snow optics assume that snow has no structures on the surfaces. For satellite ground scenes (e.g., 1km), the horizontal inhomogeneity of snow (e.g., sastrugi) may influence the snow reflectance and, therefore, the retrieved snow grain size considerably (Warren et al., 1998). We found that generally, the reflectance decreases, if sastrugi present and the decrease could be on the order of 5-30% depending on PPA (Zhuravleva and Kokhanovsky, 2011). It is smaller for smaller PPA. The patches of vegetation penetrating through snow or trees make retrievals not possible or difficult. Therefore, it is of importance to make not only cloud screening but also only 100% snow covered ground scenes (without forest and vegetation) must be used in retrievals of the grain size, snow albedo, and the concentration of snow pollutants. This is due to the fact that there is a limitation with respect to the complexity of the forward model, which can be used in the retrieval process. Although there are some reports on the retrieval of subpixel snow properties (see, e.g., Painter et al., 1998, 2003, 2009). Retrieval of snow properties in the mountainous regions is also of problem. Then effects of shadowing are evident and 3-D radiative transfer models are needed with the known topography and illumination conditions at a given location.

The retrieval of grain sizes for the polluted case (both for polluted snow and for polluted atmosphere) can cause problems if the channel at 865 nm is used for retrievals. This is due to the fact that the signal at 865 nm can be influenced by pollution (Painter et al., 2007) and this influence is difficult to assess *a priori*. For instance, there is the problem of the possible presence of soot in the atmosphere and in the snow. For longer wavelengths, the influence of pollution is reduced considerably. Although Dozier et al. (2009) report that there are cases, where the pollution (e.g., dust) influences snow reflectance at all wavelengths in the visible and near-infrared (up to $\lambda = 1.4\ \mu$m). The retrieval of the pollution level depends on the type of pollution (Warren and Wiscombe, 1980; Warren, 1982; Painter and Dozier, 2004; Painter et al., 2007). The uncertainty in the imaginary part of the ice refractive index in the visible (Warren and Brandt, 2008) can also play a role.

As noted by Peltoniemi (2007), snow becomes less reflective at larger densities of snow. The radiative transfer theory can be applied at very low densities (actually not possible for snow on ground) only and, therefore, this darkening will be interpreted as the presence of pollutants – although, in fact, the snow is fresh and clean. In particular, this could be the reason behind the observed reduction of fresh snow reflectance in the visible as compared to radiative transfer simulations (see, e.g., Fig. 7.5 Dozier et al. (2009)).

The radiative transfer model described above is valid for dry snow only. During the melting season, water can accumulate in snow. Then the model must be changed, taking into account the darkening of the snow due to the presence of liquid water in it. Modifications both of snow absorption and scattering are important. The snow grains become more spherical and grow in size. Clusters are formed (Colbeck, 1979). The presence of liquid films between grains reduces the scattering and also it leads to more extended in the forward direction phase functions. This for sure will bias retrievals if it is not accounted for in the retrieval procedure. Another possibility is the dependence of the snow bulk absorption coefficient on temperature

(e.g., for extremely low temperatures such as those possible, e.g., in the Antarctic (Grundy and Schmitt, 1998)), which is not accounted for in the current version of the algorithm. The issues highlighted above are a subject of our ongoing research on forward and inverse models in snow optics.

Acknowledgments

This work was supported by the ESA Project Snow_Radiance and also by JAXA (Japan). We thank Andreas Macke and Michael Mishchenko for providing their codes used in this study. We are grateful to ESA for providing MERIS reduced resolution data.

Appendix. The relationship between different retrieval approaches based on the asymptotic radiative transfer theory

Snow reflectance can be presented in the following way using asymptotic radiative transfer theory (Zege et al., 1991):

$$R(\mu, \mu_0, \varphi) = R_0(\mu, \mu_0, \varphi) \exp\{-pf(\mu, \mu_0, \varphi)\}, \tag{7.A1}$$

where

$$p = 4s/\sqrt{3}, s=\sqrt{\frac{1-\omega_0}{1-g\omega_0}}, f = \frac{u(\mu_0)u(\mu)}{R_0^{-1}(\mu, \mu_0, \varphi)}, u(\mu) = \frac{3}{7}(1+2\mu). \tag{7.A2}$$

Here R_0 is the reflection function of a semi-infinite snow layer under the assumption that the single scattering albedo is equal to one, the values (μ, μ_0, φ) give the cosines of observation and incidence angles, and also the relative azimuthal angle, respectively, ω_0 is the single scattering albedo, and g is the asymmetry parameter.

Various snow retrieval algorithms differ with respect to the actual implementation of Eq. (7.A1) in the retrieval code and also due to different approximations of the relationship between the similarity parameter s(or p) and a_{ef}.

Tedesco and Kokhanovsky (2007) proposed the relationship between p and the effective grain size a_{ef} in the following form:

$$p = A\sqrt{\gamma_i a_{ef}}, \tag{7.A3}$$

where $A = 5.09$, $\gamma_i = 4\pi\chi_i/\lambda$ and χ_i is the ice refractive index. The value of p can be found from Eq. (7.A1):

$$p = \frac{1}{f}\ln\left\{\frac{R_0}{R}\right\} \tag{7.A4}$$

and then the approximate solution for the function $R_0(\mu, \mu_0, \varphi)$ is used to find p, and, therefore, EGS (see Eq. (7.A3)) from the measured reflectance R at a given wavelength. The wavelength 1.24 μm is used because of the following factors:

– this reflectance at this wavelength is the most sensitive to the grain size for most situations occurring in practice;

- the influence of pollutants in snow and in the atmosphere is minimal at this wavelength;
- the retrievals have a direct meaning and relevance to the EGS at the subsurface snow layer.

A very similar method was used by Langlois et al. (2010) for the interpretation of near-infrared photography of vertical snow walls. However, they assumed that $A = 5.66$. The shortcoming of this algorithm (called SARA) is in fact that the concentration of pollutants cannot be assessed. Also the influence of pollutants on the reflectance at 1.24 μm (possible for heavy pollution events) cannot be estimated. The algorithm FORCE described in this chapter is the extension of SARA to solve this problem. Then it is assumed that p is related to a_{ef} and the concentration of soot c using the following equation, which approximately holds for the vertically homogeneous snow:

$$p = \frac{4}{\sqrt{3(1-g)}}\sqrt{\frac{2}{3}Bc\gamma_s a_{ef} + \beta_\infty(1 - \exp(-\gamma_i \kappa a_{ef}))}, \tag{7.A5}$$

where $g = 0.76$, $\kappa = 2.63$, $\beta_\infty = 0.47$, $B = 0.84$, $\gamma_s = 4\pi\chi_s/\lambda$, $\chi_s = 0.46$ is the soot refractive index in the visible (spectrally neutral) . Eq. (7.A3) follows from Eq. (7.A5) assuming that $c \equiv 0$ and $\gamma_i a_{ef} \to 0$ (but with slightly different $A = 5.24$). In this case there are two unknowns (c, a_{ef}) and they can be found, if measurements at two wavelengths are performed. In the visible, absorption by ice can be ignored and Eq. (7.A4) is used to find p, and, therefore, ca_{ef} assuming that the second term under the square root in Eq. (7.A5) can be neglected. Then p and, therefore, EGS can be found from Eqs. (7.A4), (7.A5) applied at the second wavelength (for known product $x = ca_{ef}$ determined from measurements in the visible). Finally, the soot concentration is derived as $c = x/a_{ef}$. The value of R_0 is obtained from look-up tables calculated using the Ambartsumian nonlinear integral equation. The shortcoming of this method is in the assumption that the snow grain size does not vary along the vertical.

Lyapustin et al. (2009) used the technique similar to SARA (Tedesco and Kokhanovsky, 2007). However, instead of calculations of R_0, the corresponding measured value (in the visible) was used. Such an assumption is valid in the case of pure snow (say, as in Greenland as studied by Lyapustin et al. (2009)). This makes retrievals faster and also makes it possible to account for possible errors in modeled R_0 due to possible close-packed media and 3D effects.

Finally, Zege et al. (2008) proposed the multi-channel retrieval technique based on the assumption of a vertically and horizontally homogeneous semi-infinite snow layer. In particular, they proposed to use three channels of MODIS to derive not only c and a_{ef}, but also R_0 from the measurements itself. They used Eq. (7.A1) for three wavelengths with p defined as follows:

$$p = A\sqrt{b\gamma_s c a_{ef} + \gamma_i a_{ef}}. \tag{7.A6}$$

Zege et al. (2008) used the value of A=6 in their retrievals but state that it can vary from 3.5 to 6.5 depending on snow type. It is assumed that the value of $b = 0.43$. Eq. (7.A3) follows from Eq. (7.A6) if $c = 0$. Eq. (7.A5) can be presented in the form given by Eq. (7.A6) if it is assumed that $\gamma_i a_{ef} \to 0$. The resulting constants

A and b slightly differ from those used by Zege et al. (2008) ($A = 5.24$, $b = 0.45$). More work must be done to assess the values of (A, b) from *in situ* measurements of natural snow covers.

References

Ackerman, S., Strabala, K., Menzel, P., Frey, R., Moeller, C., Gumley, L., Baum, B., Wetzel, S., Seemann, S. and Zhang, H., 2006: Discriminating clear sky from cloud with MODIS algorithm theoretical basis document (MOD35), at http://modis.gsfc.nasa.gov/data/atbd/atbd_mod06.pdf.

Aoki, T., Hori, M., Motoyoshi, H., Tanikawa, T., Hachikubo, A., Sugiura, K., Yasunari, T. J., Storvold, R., Eide, H. A., Stamnes, K., Li, W., Nieke, J., Nakajima, Y., and Takahashi, F., ADEOS-II/GLI snow/ice products – Part II, 2007: Validation results using GLI and MODIS data. *Remote Sensing of Environment*, **111**, 274–290.

Bond, T. C., and Bergstrom, R. W., 2006: Light absorption by carbonaceous particles: an investigative review, *Aerosol Science and Technology*, **40**, 27–67.

Bourdelles, B., and Fily, M., 1993: Snow grain-size determination from Landsat imagery over Terre Adelie, Antarctica, *Annals Glaciology*, **17**, 86–92.

Chandrasekhar, S., 1960: *Radiative Transfer*, New York: Dover.

Colbeck, S. C., 1979: Grain cluster in wet snow, *Journal of Colloid and Interface Sciences*, **72**, 371–384.

Colbeck, S. C., 1982: An overview of seasonal snow metamorphism, *Review of Geophysics and Space Physics*, **20**, 45–61.

Colbeck, S. C., 1983: Theory of metamorphism of dry snow, *Journal of Geophysical Research*, **88**, 5475–5482.

Colbeck, S. C., 1991: The layered character of snow covers, *Reviews of Geophysics*, **29**, 81–96.

Domine F., Albert, M., Huthwelker, T., Jacobi, H.-W., Kokhanovsky, A., Lehning, M., Picard, G., and Simpson, W. R., 2008: Snow physics as relevant to snow photochemistry, *Atmospheric Chemistry and Physics*, **8**, 171–208.

Dozier, J., 1987: Recent research in snow hydrology, *Reviews of Geophysics*, **25**(2), 153–161.

Dozier, J., and Painter, T. H., 2004: Multispectral and hyperspectral remote sensing of alpine snow properties, *Annual Review of Earth and Planetary Sciences*, **32**, 465–494.

Dozier, J., Green, R.O., Nolin, A. W., and Painter, T. H., 2009: Interpretation of snow properties from imaging spectrometry, *Remote Sensing of Environment*, **113**, S25–S37.

Fily, M., Bourdelles, B., Dedieu J. P., and Sergent, C., 1997: Comparison of in situ and Landsat Thematic Mapper derived snow grain characteristics in the Alps, *Remote Sensing of Environment*, **59**, 452–460.

Flanner, M. G., Zender, C. S., Randerson, J. T., Rasch, P. J., 2007: Present-day climate forcing and response from black carbon in snow, *Journal of Geophysical Research*, **112**, D11202, doi:10.1029/2006JD008003.

Gallet, J.-C., Domine, F., Zender, C. S., and Picard G., 2009: Measurements of the specific surface area of snow using infrared reflectance in an integrating sphere at 1310 and 1550 nm, *Cryosphere*, **3**, 167–182,

Garret, T. J., Hobbs, P.V., and Gerber, H., 2001: Shortwave, single scattering properties of arctic ice clouds, *Journal of Geophysical Research*, **106**, D14, 15,555–15,172.

Grundy W. M., and Schmitt B., 1998: The temperature-dependent near-infrared absorption spectrum of hexagonal H_2O ice, *Journal Geophysical Research*, **103**, E11, 25809–25822.

Hansen J., and Nazarenko L., 2004: Soot climate forcing via snow and ice albedos, *Proceedings of National Academy of Sciences of USA*, **101**, 423–428.

Hori, M., Aoki, T., Stamnes, K., and Li, W., 2007: ADEOS-II/GLI snow/ice products – Part III: Retrieved results, *Remote Sensing of Environment*, **111**, 291–336.

Kokhanovsky, A. A., 1998: On light scattering in random media with large densely packed particles, *Journal of Geophysical Research*, **103**(D6), 6089–6096.

Kokhanovsky, A. A., and Nauss, T., 2005: Satellite based retrieval of ice cloud properties using semianalytical algorithm, *Journal of Geophysical Research*, **110**, D19206, doi: 10.1029/2004JD005744, 2005.

Kokhanovsky, A. A., and Schreier, M., 2008: The determination of snow albedo using combined AATSR and MERIS observations, in Proc. of the 2nd MERIS/(A)AATSR Workshop, Frascati, Italy, 22–26 September 2008 (ESA SP-666, November 2008).

Kokhanovsky, A. A., and Schreier M., 2009: The determination of snow specific area, albedo and effective grain size using AATSR spaceborne observations, *International Jounal Remote Sensing*, **30**, 4, 919–933.

Kokhanovsky, A. A., and Zege, E. P., 2004: Scattering optics of snow, *Applied Optics*, **43**, 1589–1602.

Kokhanovsky, A. A., Aoki, T., Hachikubo, A., Hori, M., and Zege, E. P., 2007: Reflective properties of natural snow: approximate asymptotic theory versus in situ measurements, *IEEE Transactions on Geosciences and Remote Sensing*, **43**, 1529–1535.

Kokhanovsky, A. A., Rozanov V., Aoki T., et al., 2011: Sizing snow grains using backscattered solar light, *International Journal Remote Sensing*, in press.

Langlois, A., Royer, A., Motpetit, B., et al., 2010: On the relationship between snow grain morphology and in situ near infrared calibrated reflectance photographs, *Cold regions Science and Technology*, **61**, 34–42.

Legagneux, L., Cabanes, A., and Domine, F., 2002: Measurement of the specific surface area of 176 snow samples using methane adsorption at 77 K, *Journal of Geophysical Research*, **107** (D17), 4335, doi: 10.1029/2001JD001016.

Lenoble, J., 1985: *Radiative Transfer in Scattering and Absorbing Atmospheres: Standard Computational Procedures*, Hampton: Deepak.

Li, W., Stamnes, K., Chen, B., and Xiong, X., 2001: Snow grain size retrieved from near-infrared radiances at multiple wavelengths, *Geophysical Research Letters*, **28**, 1699–1702, doi: 10.1029/2000GL011641.

Lyapustin. A., Tedesco, M., Wang, Y., Aoki, T., Hori, M., and Kokhanovsky, A., 2009: Retrieval of snow grain size over Greenland from MODIS, *Remote Sensing of Environment*, **113**, 1976–1987.

Macke, A., J. Mueller, E. Raschke, 1996: Single scattering properties of atmospheric ice crystals, *Journal Atmospheric Science*, **53**, 2813–2825.

Matzl, M., 2006: Quantifying the stratigraphy of snow profiles, PhD Thesis, Swiss Federal Institute of Technology, Zürich.

Matzl, M., and Schneebeli,M., 2006: Measuring specific surface area of snow by near-infrared photography, *Journal of Glaciology*, **52**, 558–564.

Mishchenko, M. I., Dlugach, J. M., Yanovitskij, E. G., and Zakharova, N. T., 1999: Bidirectional reflectance of flat, optically thick particulate layers: an efficient radiative transfer solution and applications to snow and soil surfaces, *Journal of Quantitative Spectroscopy and Radiative Transfer*, **63**, 409–432.

Muinonen, K., Nusiainen, T., Fast, P., Lumme, K., and Peltoniemi, J. I., 1996: Light scattering by Gaussian random particles: ray optics approximation, *Journal of Quantitative Spectroscopy and Radiative Transfer*, **55**, 577–601.

Nolin, A.W., and Dozier, J., 1993: Estimating snow grain size using AVIRIS data, *Remote Sensing of Environment*, **44**, 231–238.

Nolin, A. W., and Dozier, J., 2000: A hyperspectral method for remotely sensing the grain size of snow, *Remote Sensing of Environment*, **74**, 207– 216.

Nolin, A. W., and Liang, S., 2000: Progress in bidirectional reflectance modeling and applications for surface particulate media: snow and soils, *Remote Sensing Reviews*, **18**, 307–342.

Odermatt D., Schläpfer, D., Lehning, M., Schwikowski, M., Kneubühler, M., and Itten, I. K., 2005: Seasonal study of directional reflectance properties of snow, EARSeL eProceedings, 4, 203–214.

Painter, T. H., Dozier, J., Roberts, D. A., Davis, R. E., and Greene, R. O., 2003: Retrieval of subpixel snow-covered area and grain size from imaging spectrometer data, *Remote Sensing of Environment*, **85**, 64–77.

Painter, T. H., Roberts, D. A., Green, R. O., and Dozier, J., 1998: The effect of grain size on spectral mixture analysis of snow-covered area from AVIRIS data, *Remote Sensing of Environment*, **65**, 320–332.

Painter, T. H., and Dozier, J., 2004: Measurements of the hemispherical–directional reflectance of snow at fine spectral and angular resolutions, *Journal of Geophysical Research*, **109**, doi: 10.1029/2003JD004458.

Painter T. H., Barrett, A. P., Landry, C. C., Neff, J. C., Cassidy, M. P., Lawrence, C. R., McBride, K. E., and Farmer, G. L., 2007: Impact of disturbed desert soils on duration of mountain snow cover, *Geophysical Research Letters*, **34**, L12502, doi:10.1029/2007GL030284.

Painter, T. H., Rittger, K., McKenzie, C., Slaughter, P., Davis, R. E., and Dozier, J., 2009: Retrieval of subpixel snow covered area, grain size, and albedo from MODIS, *Remote Sensing of Environment*, **113**, 868–879.

Polonsky, I. N., Zege, E. P., Kokhanovsky, A. A., Katsev, I. L., and Prikhach, A. S., 1999: The retrieval of the effective radius of snow grains and control of snow pollution with GLI data, Geoscience and Remote Sensing Symposium, IGARSS '99 Proceedings, IEEE 1999 International, 2, 28 June–2 July 1999, pp. 1071–1073 vol. 2, DOI: 10.1109/IGARSS.1999.774536.

Rozanov, A. A., Rozanov, V. V., Buchwitz, M., Kokhanovsky, A. A., and Burrows, J. P., 2005: SCIATRAN 2.0-a new radiative transfer model for geophysical applications in the 175–2400 nm spectral range, *Advances in Space Research*, **36**, 1015–1019.

Rozanov, V. V., Rozanov, A. V., and Kokhanovsky, A. A., 2007: Derivatives of the radiation field and their application to the solution of inverse problems, in A. A. Kokhanovsky (ed.), *Light Scattering Reviews*, vol. 2, pp. 205–265, Chichester, UK: Praxis.

Sandmeier, S. R., and Itten, K. I., 1999: A field goniometer system (FIGOS) for acquisition of hyperspectral BRDF data, *IEEE Transactions on Geoscience and Remote Sensing*, **37**, 978–986.

Schneebeli, M., and Sokratov, S. A., 2004: Tomography of temperature gradient metamorphism of snow and associated changes in heat conductivity, *Hydrological Processes*, **18**, 3655–3665.

Stamnes, K., Li, W., Eide, H., Aoki, T., Hori, M., and Storvold, R., 2007: ADEOS-II/GLI snow/ice products – Part I: Scientific basis, *Remote Sensing of Environment*, **111**, 258–273.

Tanikawa, T., Aoki, T., Hori, M., Hachikubo, A., and Aniya, M., 2006: Snow bidirectional reflectance model using nonspherical snow particles and its validation with field measurements, *EARSeL Proceedings*, **5**, 137–145.

Tedesco, M., and Kokhanovsky A. A., 2007: The semi-analytical snow retrieval algorithm and its application to MODIS data, *Remote Sensing of Environment*, **110**, 317–331.

Tomasi, C., Vitale, V., and Lupi, A., 2007: Aerosols in polar regions: A historical overview based on optical depth and in situ observations, *Journal of Geophysical Research*, **112**, D16205, doi: 10.1029/2007JD008432.

van de Hulst, H. C., 1957: *Light Scattering by Small Particles*, New York: John Wiley.

Warren, S. G., 1982: Optical properties of snow, *Reviews of Geophysics*, **20**, 67–89.

Warren, S. G., 1984: Optical constants of ice from the ultraviolet to the microwave. *Applied Optics*, **23**, 1206–1225.

Warren S. G., and Brandt, R. E., 2008: Optical constants of ice from the ultraviolet to the microwave: A revised compilation, *Journal of Geophysical Research*, **113**, D14220, doi:10.1029/2007JD009744.

Warren, S. G., and Wiscombe, W. J., 1980: A model for the spectral albedo of snow. II: Snow containing atmospheric aerosols. *Journal of Atmospheric Sciences*, **37**, 2734–2733.

Warren, S. G., Brandt, R. E., and Hinton, P., 1998: Effects of surface roughness on bidirectional reflectance of Antarctic snow, *Journal of Geophysical Research*, **103**, 25789–25807.

Xie, Y., Yang, P., Gao, B.-C., Kattawar, G. W., and Mishchenko, M. I., 2006: Effect of ice crystal shape and effective size on snow bidirectional reflectance, *Journal of Quantitative Spectroscopy and Radiative Transfer*, **100**, 457–469.

Zege, E. P., Ivanov A. P., and Katsev, I. L., 1991: Image transfer through a scattering medium, Berlin: Springer.

Zege, E. P., Kokhanovsky, A. A., Katsev, I. L., Polonsky, I. N., and Prikhach, A. S., 1998: The retrieval of the effective radius of snow grains and control of snow pollution with GLI data, in Proceedings of Conference on Light Scattering by Nonspherical Particles: Theory, Measurements, and Applications, Mishchenko, M. I., Travis, L. D., and Hovenier, J. W., eds. American Meteorological Society, Boston, MA, 288–290.

Zege, E. P., Katsev, I. L., Malinka, A., Prikhach, A. S., and Polonsky, I. N., 2008: New algorithm to retrieve the effective snow grain size and pollution amount from satellite data, *Annals of Glaciology*, **49**, 139–144.

Zhou, X., Li, S., and Stamnes, K., 2003: Effects of vertical inhomogeneity on snow spectral albedo and its implications for remote sensing of snow, *Journal of Geophysical Research*, **108**, 4738, 2003. doi: 10.1029/2003JD003859.

Zhuravleva, T., and Kokhanovsky, A., 2011: Influence of surface roughness on the reflective properties of snow, *J. Quant. Spectr. Rad. Transfer*, submitted.